A partner switch from CDS2 to RAB1A redirects MBOAT7 to inhibit DGAT2-mediated lipid droplet growth

Jiesi Xu[1, 2, 3, *], Jianxin Zhang[3, 4, *], Wei Wang[3], Honggang Su[3, 4], Siyu Chen[5], Mei Ding[2, 3] and Xun Huang[2, 3, 6, #]

1. The Key Laboratory of Geriatrics, Beijing Institute of Geriatrics, Institute of Geriatric Medicine, Chinese Academy of Medical Sciences, Beijing Hospital/National Center of Gerontology of National Health Commission, Beijing, 100730, China

2. State Key Laboratory of Metabolism and Regulation in Complex Organisms, Taikang Center for Life and Medical Sciences, School of Basic Medical Sciences, Wuhan University, Wuhan, Hubei 430071, China

3. Institute of Genetics and Developmental Biology, Chinese Academy of Sciences, Beijing 100101, China

4. University of Chinese Academy of Sciences, Beijing 100049, China

5. Medical Research Center, Beijing Institute of Respiratory Medicine and Beijing Chao-Yang Hospital, Capital Medical University, Beijing 100020, China

6. Tianjian Laboratory of Advanced Biomedical Sciences, Zhengzhou University, Zhengzhou 450001, China

* Equal contribution

To whom correspondence should be addressed at: State Key Laboratory of Metabolism and Regulation in Complex Organisms, Taikang Center for Life and Medical Sciences, School of Basic Medical Sciences, Wuhan University, Wuhan, Hubei 430071, China

Email: huangxun@whu.edu.cn; xhuang@genetics.ac.cn

Abstract

Metabolic dysfunction-associated steatotic liver disease (MASLD) is a highly prevalent disorder worldwide characterized by the accumulation of hepatic lipid droplets (LDs). However, the mechanisms by which hepatocytes adapt to the dynamic changes in LD morphology to maintain metabolic homeostasis remains incompletely understood. Here, we show that MBOAT7, a known MASLD-associated protein, cooperates with CDS2 to regulate lipid droplet dynamics and lipid metabolism. Under physiological conditions, their interaction in the endoplasmic reticulum (ER) maintains metabolic homeostasis. Disruption of this interaction, such as through CDS2 knockdown or loss of function, triggers an adaptive response wherein MBOAT7 translocates to ER-LD contact sites in a RAB1-dependent manner. This redistribution inhibits DGAT2-mediated LD growth and promotes lipolysis. Our findings highlight the redistribution of MBOAT7 to ER-LD contacts serves as a critical mechanism for adaptive control LD size and lipid metabolic homeostasis.

Introduction

The liver serves as the central hub for systemic lipid metabolism, orchestrating the complex processes of fatty acid synthesis, storage, and mobilization, as well as cholesterol homeostasis. Disruptions in this delicate equilibrium are a hallmark of metabolic dysfunction-associated steatotic liver disease (MASLD), a burgeoning global health concern that can progress from simple hepatic steatosis to steatohepatitis (MASH), fibrosis, and cirrhosis (1).

The excessive accumulation of hepatic lipid droplets (LDs) is a central pathological feature of MASLD (2). As dynamic organelles, LDs serve as key hubs for neutral lipid storage and metabolism, and their formation acts as a compensatory mechanism to protect hepatocytes from cytotoxic free fatty acids and other bioactive lipids. However, while initially adaptive, persistent LD expansion causes physical distortion of hepatocytes, nuclear displacement, and alterations in liver parenchymal architecture (3-5). Although the triggers and consequences of hepatic LD accumulation in MASLD have been extensively studied, how hepatocytes actively counteract and mitigate the increasing LD expansion remains incompletely understood. Two major adaptive strategies have emerged: first, lipolysis and lipophagy, which preferentially target smaller LDs that are more accessible for degradation (6, 7); and second, remodeling of inter-organelle contacts between LDs and other organelles—such as the endoplasmic reticulum, mitochondria, and lysosomes, facilitating lipid processing and degradation (8, 9). Through these mechanisms, LD remodeling serves as a vital process for maintaining metabolic homeostasis. LD-associated proteins are known to regulator of LD size, yet their specific roles in counteracting LD expansion await further elucidation.

A critical, yet often overlooked, aspect of hepatic lipid regulation is the spatial organization of metabolic enzymes within cellular organelles and the dynamic contact sites between them, particularly those between the endoplasmic reticulum (ER) and lipid droplets (LDs). These ER-LD contact sites are emerging as vital platforms for lipid trafficking, synthesis, and signaling (8, 10-13), but the molecular mechanisms that govern protein targeting to these sites and their functional consequences for

whole-body metabolism remain incompletely understood.

Membrane Bound O-Acyltransferase Domain Containing 7 (MBOAT7) and CDP-Diacylglycerol Synthase (CDS) are two enzymes implicated in distinct branches of phospholipid metabolism. MBOAT7, an ER-resident enzyme, incorporates polyunsaturated fatty acids into lysophosphatidylinositol through the PI remodeling Lands' cycle (14), and its loss-of-function variants in humans are strongly associated with an increased risk of MASLD, liver fibrosis, and hepatocellular carcinoma (15-18). Parallel to this pathway, PI can also be synthesized *de novo* via the Kennedy pathway, in which the conversion of phosphatidic acid to CDP-diacylglycerol (CDP-DAG) by CDS (CDP-DAG synthase) constitutes a critical step (19, 20). Notably, CDS2, one of the two CDS proteins in mammals, is selectively inhibited by arachidonoyl-containing PI species (PI-AA), suggesting a regulatory feedback loop that links MBOAT7-mediated PI remodeling with CDS2-mediated *de novo* PI synthesis (21). This interplay is biologically significant: *Mboat7* deficiency has been shown to promote hepatic lipid accumulation and steatohepatitis, partly through increasing CDS2 activity (22, 23). Conversely, deletion of *Cds2* leads to the formation of large LDs and spontaneous development of metabolic dysfunction-associated steatohepatitis (MASH) (24-26), providing a valuable model for studying hepatocyte adaptations to drastic LD morphological changes. While the individual roles of these enzymes in their respective biochemical pathways are recognized, a broader, integrative understanding of how they might functionally interact to coordinate hepatic lipid flux has been lacking.

Here, we uncover a coordinated mechanism by which MBOAT7 and CDS2 jointly regulate LD dynamics. We demonstrate that *CDS2* deletion triggers the adaptive relocation of MBOAT7 to ER-LD contact sites, where it restricts LD expansion by competing with RAB1-mediated DGAT2 targeting to LD. These findings establish MBOAT7 and CDS2 as key regulators of a membrane-metabolic crosstalk that integrates inter-organelle communication with lipid homeostasis, revealing a robust adaptive response to hepatic steatosis in hepatocytes.

Results

MBOAT7 is localized to the ER-LD contacts in lipid-loaded *CDS2* KO cells

We have previously shown that *Cds2* deficiency causes a rapid development of MASH (26). To explore the cellular function of CDS2, we conducted APEX2-based proximity labeling using an APEX2-CDS2 fusion protein to identify its proximal partners (Figure S1A). Across two biological replicate experiments, we identified 24 proteins specifically enriched in APEX2-CDS2-expressing cells compared to APEX2 alone control. Given the ER localization of CDS2, we focused on ER-associated proteins (Figure S1B). Among these, MBOAT7 emerged as a protein of particular interest due to its established role in phosphatidylinositol biosynthesis and its associated with MASLD. Therefore, we chose MBOAT7 for further investigation.

To investigate the functional interplay between MBOAT7 and CDS2, we first studied whether their enzymatic activities were affected by each other. Previous report show that the activity of CDS2 is selectively inhibited by arachidonoyl-containing PI species (PI-AA), the product of MBOAT7-mediated PI remodeling (21). Therefore, we measured whether CDS2 affects the acyltransferase activity of MBOAT7 using MBOAT7 substrates, lyso-PI and [14C]-arachidonic acid. We analyzed the activity of MBOAT7 in the ER from the liver of control mice (*Cds2*$^{f/f}$), mice with liver-specific depletion of *Cds2* (*Cds2*$^{f/f}$*;AlbCre*), and hepatic *Cds2*-depleted mice with AAV-mediated hepatic re-expression of *Cds2* (*Cds2*$^{f/f}$*;AlbCre* + AAV-TBG-*Cds2*). The results showed that *Cds2* deficiency did not significantly impact the enzymatic activity of MBOAT7 (Figure 1A).

Previous studies have shown that *CDS2* knockout induced large LDs (25). Given the shared subcellular localization and functional interplay between MBOAT7 and CDS2, we sought to investigate the localization and roles of MBOAT7 in LD regulation. MBOAT7-EGFP exhibited an ER-like localization pattern in both wild-type and *CDS2* KO HeLa cells (Figure S2A and B). Interestingly, in *CDS2* KO cells treated with oleic acid (OA) to induce LD formation, MBOAT7-EGFP surrounded LDs stained by LipidTOX (Figure 1B-C). In contrast, MBOAT7-EGFP did not show colocalization with LDs in OA-treated control HeLa cells (Figure 1B-C).

134 Furthermore, in OA-treated *CDS2* KO cells, MBOAT7-EGFP was colocalized with
135 the LD marker mScarlet-PLIN1, whereas no such colocalization was observed in
136 control cells (Figure S2C). Similarly, in OA-treated HepG2 cells, MBOAT7-EGFP
137 remained localized to the ER, but enclosed LDs when *CDS2* was knocked down
138 (Figure S1D). To rule out the possibility that the phenomena is caused by EGFP
139 tagging, we also analyzed the localization of endogenous MBOAT7. In OA-treated
140 *CDS2* KO cells, endogenous MBOAT7 colocalized with LDs, but this was not
141 observed in OA-treated control cells (Figure 1D-E). We also notice that under these
142 conditions, the MBOAT7 protein surrounding the LD surface is often incomplete,
143 with one or more nicks (Figure 1D arrow).
144 There are several mechanisms for protein localization on the LDs, including short
145 hairpin, hydrophobic region (which may form an amphipathic helix), and lipid
146 modification (27). Since MBOAT7 is a multipass transmembrane protein, it is likely
147 localized to ER regions adjacent to LDs rather than directly to the LD phospholipid
148 monolayer. Indeed, 3D reconstruction of the LDs confirmed that MBOAT7 partially
149 surrounds the LDs in OA-treated *CDS2* KO cells (Figure 1F).
150 The observed targeting of ER-localized MBOAT7 to the ER-LD contacts in
151 *CDS2* KO cells prompted us to investigate whether *CDS2* depletion affects the
152 targeting of other ER proteins to LDs. The ER marker mScarlet-SEC61b did not
153 colocalize with LDs in OA-loaded *CDS2* KO HeLa cells (Figure 1G-H). Next, we
154 examine whether this relocalization of MBOAT7 to ER-LD is related to MASH
155 pathogenesis. Since CDS2 protein levels are downregulated in MASH mouse models
156 (26), we also examined MBOAT7 localization in the liver of the
157 fat/fructose/cholesterol-rich Gubra-Amylin NASH (GAN) diet feeding-induced
158 MASH mice. Confocal imaging showed that endogenous MBOAT7 was more
159 enriched at the LD periphery in liver sections from GAN diet-induced MASH mice
160 compared to those from normal mice (Figure 1I-J). These findings suggest that
161 MBOAT7 specifically localizes to the ER-LD contacts in lipid-overloaded
162 *CDS2*-deficient cells but not in control cells.
163 MBOAT7 consists of 11 transmembrane (TM) helices organized into two bundles

164 (TM1-5 and TM9-11) that tilt apart, creating a central catalytic chamber (28) (Figure
165 1K). To identify the region required for the localization of MBOAT7 to the ER-LD
166 contacts, we generated three EGFP-tagged truncated versions of MBOAT7,
167 containing the N-terminal region (amino acids 1-135), the central region (180-310),
168 and the C-terminal region (311-472) (Figure 1K). Only the N-terminal region
169 localized to the ER-LD contacts in *CDS2* KO cells, and MBOAT7 with a deletion of
170 the N-terminal 99 amino acids did not localize to the ER-LD contacts (Figure 1L).
171 Therefore, the N-terminus of MBOAT7 is required for the localization of MBOAT7 to
172 ER-LD contacts in *CDS2* KO cells.
173
174 **MBOAT7 interacts with CDS2**
175 Next, we investigated the mechanism underlying MBOAT7 localization to ER-LD
176 contact sites specifically in *CDS2* KO cells. Since both CDS2 and MBOAT7 are
177 localized to the ER and MAMs (26) and MBOAT7 is found in CDS2 proximal
178 proteome, we hypothesized that CDS2 retains MBOAT7 within the ER, while
179 MBOAT7 relocates to the ER-LD contacts upon *CDS2* depletion. To test this, we
180 performed co-immunoprecipitation (co-IP) assays, which show that Flag-CDS2
181 precipitated MBOAT7-EGFP (Figure 2A), and, reciprocally, MBOAT7-EGFP
182 precipitated Flag-CDS2 (Figure 2B). To rule out potential artifacts from protein
183 overexpression, we used CRISPR-based knock-in (KI) to tag the endogenous CDS2
184 locus with an N-terminal EGFP and confirmed that endogenous CDS2 coprecipitated
185 with endogenous MBOAT7 in HeLa cells (Figure 2C). To examine the direct binding
186 between these two proteins, we purified His-MBOAT7 from E. coli and Flag-CDS2
187 from mammalian cells. Western blot analysis confirmed their direct interaction
188 (Figure 2D). Collectively, these results demonstrate the interaction between CDS2 and
189 MBOAT7, which retains MBOAT7 at the ER.
190
191 **RAB1A regulates the localization of MBOAT7 at the ER-LD contacts in *CDS2***
192 **KO cells**
193 Next, we investigated how MBOAT7 is recruited to the ER-LD contacts in *CDS2* KO

194 cells. ER proteins typically target the LD monolayer surface, which requires
195 membrane continuity between the ER outer leaflet and the LD monolayer (11). This
196 targeting can occur either during early LD formation or to mature LDs after their
197 formation. These ER proteins associate with the LD monolayer through hydrophobic
198 hairpins, which insert midway into the lipid bilayers of the ER, with both the N- and
199 C-termini facing the cytosol (29). Since MBOAT7 lacks a hairpin structure, we
200 hypothesized that ER-localized MBOAT7 associates with LDs in *CDS2* KO cells via
201 interaction with LD-associated proteins.

202 We conducted an unbiased proteomic screen for MBOAT7-interacting proteins in
203 *CDS2* KO Hela cells. We immunoprecipitated MBOAT7-EGFP from control and
204 *CDS2* KO cells and identified its interacting proteins using LC-MS/MS (Figure 3A).
205 We hypothesized that MBOAT7 would interact with LD proteins in *CDS2* KO cells
206 but not in control cells, so we selected candidates whose interaction with MBOAT7 in
207 *CDS2* KO cells was at least 2-fold stronger than in control cells. Based on previously
208 published LD proteomes (30-32), we focused on LD proteins. Five proteins from our
209 dataset were shared with all the published LD proteomes (Figure 3B). Interestingly, of
210 these five candidates, four of them are RAB proteins (RAB1A, RAB7A, RAB14 and
211 RAB18) (Figure 3C). Previous studies reported that RAB1 mediates targeting
212 triglyceride biosynthetic enzymes to LDs (13, 33). Our results showed that
213 knockdown of *RAB1A* impaired the LD targeting of MBOAT7 in OA-loaded *CDS2*
214 KO cells (Figure 3D-F). To determine whether this regulatory relationship involves a
215 direct physical interaction, co-IP assays showed that MBOAT7-EGFP interacted with
216 Flag-RAB1A in *CDS2* KO cells but not in control cells, suggesting that RAB1A helps
217 MBOAT7 target to the ER-LD contacts in *CDS2* KO cells (Figure 3G). Furthermore,
218 expressing HA-tagged CDS2 in *CDS2* KO cells inhibited the interaction between
219 MBOAT7 and RAB1A (Figure 3H).

220 We then determined the binding sites between MBOAT7 and RAB1A. MBOAT7
221 structure were shown previously (28). The crystal structure of RAB1A was predicted
222 using AlphaFold3, and the 3D structure of MBOAT7/RAB1A docking was simulated.
223 The results showed that the amino acid residues F134, S135, E178 in MBOAT7 and

224 the amino acid residues F73, Y80, K90 in RAB1A were the potential interaction sites
225 (Figure 3I). Mutation of the predicted binding sites within MBOAT7 to alanine
226 abrogated their interaction (Figure 3J). Together, these results support a model of a
227 regulated partner switch: CDS2 retains MBOAT7 in the ER by competing with
228 RAB1A, but upon *CDS2* depletion, RAB1A binds MBOAT7 and recruits it to ER-LD
229 contact sites.
230
231 **MBOAT7 reduces LD size in *CDS2* KO cells by inhibiting the targeting of**
232 **DGAT2 to LDs**
233 We then investigated the cellular and physiological functions of ER-LD
234 contact-localized MBOAT7. Overexpression of MBOAT7-EGFP did not affect LD
235 size in control cells, but it reduced LD size in *CDS2* KO cells (Figure 4A-B).
236 Overexpression of an MBOAT7 mutant with reduced catalytic activity
237 (MBOAT7(N321A, H356A)-EGFP) still reduced the LD size in *CDS2* KO cells
238 (Figure 4A-B). This indicates that the effect of MBOAT7 on LD size reduction in
239 *CDS2* KO cells is independent of its enzymatic activity.
240 To explore the underlying mechanism, we considered previous findings
241 suggesting that the lipid biosynthetic enzymes DGAT2 and GPAT4 target LDs earlier
242 in *CDS2* KO cells than in control cells, promoting LD growth (24). Knockdown of
243 DGAT2 or GPAT4 reduced the LD size in *CDS2* KO cells (24). Recent evidence
244 suggests that RAB1B, which has highly similar amino acid sequences with RAB1A,
245 is required for trafficking the triglyceride-synthesizing enzyme DGAT2 to LDs in
246 mammalian cells (33). *Drosophila* RAB1 is essential for targeting ER proteins to LDs
247 (13). We hypothesized that MBOAT7 may act as a competitive inhibitor of RAB1A.
248 Specifically, we hypothesized that MBOAT7 could restrict LD expansion in *CDS2*
249 KO cells by competing with DGAT2 or GPAT4 for RAB1A binding, thereby
250 interfering with their LD targeting. In line with this hypothesis,
251 co- immunoprecipitation assays confirmed that both Flag- DGAT2 and Flag- GPAT4
252 interact with GFP- tagged RAB1A (Figure 4C and D). Interestingly, although
253 MBOAT7 overexpression did not affect the binding between GPAT4 and RAB1A

254 (Figure 4E), it significantly reduced the interaction between Flag- DGAT2 and
255 GFP- RAB1A in *CDS2* KO cells (Figure 4F). When the interaction between MBOAT7
256 and RAB1A is disrupted, the binding between Flag-DGAT2 and GFP-RAB1A is
257 retained (Figure 4F). Conversely, knockdown of MBOAT7 enhanced the binding
258 between Flag-DGAT2 and GFP-RAB1A in *CDS2* KO cells (Figure 4G). To determine
259 whether this regulated interaction translates to functional consequences in
260 cells, confocal images showed that EGFP-DGAT2 was targeted to LDs in *CDS2* KO
261 cells, but overexpression of MBOAT7-mCherry blocked this targeting (Figure 4H).
262 These results collectively demonstrate that MBOAT7 specifically modulates the
263 DGAT2-RAB1A interaction in a dose-dependent manner.
264 In response to OA treatment, triglyceride synthesis enzymes like DGAT2 or
265 GPAT4 are more likely to target to LDs to promote LD growth (34). We also tested
266 whether OA treatment affects the interaction of these enzymes with RAB1. OA
267 treatment enhanced DGAT2 binding to RAB1A but did not affect GPAT4 binding to
268 RAB1A (Figure 4I and Figure S2E). Interestingly, MBOAT7 binding to RAB1A
269 increased after OA treatment in *CDS2* KO cells (Figure 4J). Taken together, our data
270 suggest that CDS2 retains MBOAT7 at the ER. When CDS2 is absent, MBOAT7
271 binds to RAB1A and localizes to the ER-LD contacts. Furthermore, MBOAT7
272 reduces the size of LDs by reducing the targeting of DGAT2 to LDs.
273
274 **MBOAT7 and CDS2 coordinately regulate hepatic cholesterol excretion and**
275 **fatty acid synthesis**
276 The above results demonstrated that MBOAT7 and CDS2 regulate LD size in cells.
277 Next, we examined how MBOAT7 and CDS2 functionally interact and regulate LD
278 size *in vivo*. To define the coordinated roles of these enzymes in hepatic lipid
279 metabolism, we performed genetic knockdown and overexpression studies in mice.
280 We specifically single and double knocked down these enzymes in the liver, by
281 injecting C57BL/6 mice with AAV-TBG-sh*Mboat7*, AAV-TBG-sh*Cds2* or
282 AAV-TBG-sh*Mboat7*+AAV-TBG-sh*Cds2* (Figure 5A). Consistent with previous
283 report (35), knockdown of *Mboat7* in liver did not affect plasma lipid content but

284 increased hepatic triglyceride and cholesterol content (Figure 5B-E). Similarly,
285 knockdown of *Cds2* did not affect plasma triglyceride content, but increased plasma
286 and hepatic cholesterol and hepatic triglyceride content (Figure 5B-E). Interestingly,
287 knockdown of both *Mboat7* and *Cds2* did not exert additive effects on the increased
288 lipid levels, suggesting that they likely operate within the same regulatory network.
289 The triglyceride and cholesterol contents were compatible to single knockdowns
290 (Figure 5B-E). Consistent with the above results, H&E staining showed that
291 knockdown of *Mboat7*, *Cds2*, and *Mboat7* + *Cds2* increased hepatic steatosis (Figure
292 5F-G).

293 To examine the pathways regulated by MBOAT7 and CDS2, we performed RNA
294 sequencing (RNAseq) analysis on liver from the sh*Mboat7*, sh*Cds2*, and sh*Mboat7* +
295 sh*Cds2* groups. When we compared the results, we noticed an extensive overlap
296 between the three datasets: 266 genes were significantly upregulated and 301 genes
297 were significantly downregulated in all three groups (Figure 5H). Kyoto Encyclopedia
298 of Genes and Genomes (KEGG) analysis revealed significant changes in cholesterol
299 and fatty acid metabolism pathways among the genes with downregulated expression
300 in all three groups (Figure 5I). For the genes with upregulated expression in all three
301 groups, KEGG analysis revealed significant alterations in steroid biosynthesis and
302 non-alcoholic fatty liver pathways (Figure 5J).

303 LXR, a key regulator of cholesterol efflux, controls the transcription levels of
304 genes such as *Abca1* and *Abcg5/8*. Our qPCR analysis verified that genes involved in
305 cholesterol excretion (*Lxr, Abcg8* and *Abca1*) were downregulated in liver (Figure 5K),
306 indicating that reduced expression of *Mboat7* or *Cds2* impairs cholesterol excretion.
307 Knockdown of *Mboat7* and *Cds2* increased the expression of *Fasn*, which regulates
308 fatty acid biosynthesis (Figure 5K). Accordingly, LXR protein levels were reduced in
309 the liver of sh*Mboat7*, sh*Cds2*, and sh*Mboat7*+sh*Cds2* mice (Figure 5L-M). Nuclear
310 SREBP2 and HMGCR levels were diminished, likely due to feedback inhibition of
311 cholesterol biosynthesis by increased cellular cholesterol levels (Figure 5L-M).
312 Together, these data suggests that MBOAT7 and CDS2 function in a coordinated
313 way to orchestrate hepatic lipid metabolism.

314

315 **MBOAT7 regulates LD size and lipolysis in the absence of CDS2**

316 Next, we examined whether MBOAT7 overexpression is able to reduce *Cds2*
317 depletion-caused steatosis *in vivo*. *Cds2*$^{f/f}$ and *Cds2*$^{f/f}$*;AlbCre* mice were injected with
318 AAV-TBG-Con or AAV-TBG-*Mboat7* to specifically express *Mboat7* in liver (Figure
319 6A). Cell fractionation assays revealed that overexpression of *Mboat7* reduced the
320 protein level of DGAT2 in the LD fraction from the livers of *Cds2*$^{f/f}$*;AlbCre* mice,
321 while increasing the protein level of ATGL (also called PNPLA2) (Figure 6B), a
322 rate-limiting enzyme for lipolysis. This observation is consistent with our findings in
323 cultured cells (Figure 4H), where MBOAT7 disrupted DGAT2 localization to LDs.
324 The concurrent upregulation of ATGL further suggests that MBOAT7 expression may
325 actively shift lipid metabolic balance toward lipolysis. To test if MBOAT7 regulates
326 lipolysis, we used isoprenaline (ISO) to stimulate lipolysis. The results showed that
327 overexpression of MBOAT7 increased free fatty acid (FFA) release in both DMSO
328 and ISO-treated *Cds2*-deficient primary hepatocytes (Figure 6C).

329 Hepatic overexpression of *Mboat7* did not affect plasma lipids in either control or
330 *Cds2*$^{f/f}$*;AlbCre* mice (Figure 6D-E). Hepatic overexpression of *Mboat7* did not change
331 hepatic triglyceride and cholesterol levels in *Cds2*$^{f/f}$ mice, but it reduced hepatic
332 triglyceride and cholesterol levels in *Cds2*$^{f/f}$*;AlbCre* mice (Figure 6F-G). H&E
333 staining showed that liver sections from *Cds2*$^{f/f}$*;AlbCr*e mice contained "supersized"
334 LDs, while overexpression of *Mboat7* reduced the LD size in *Cds2*$^{f/f}$*;AlbCre* mice,
335 resulting in multiple small-sized LDs in hepatocytes (Figure 6H). This reduction in
336 LD size was also confirmed in *Cds2*-deficient primary hepatocytes (Figure 6I-J).
337 Overall, our data suggest that MBOAT7 controls LD size and lipolysis by inhibiting
338 DGAT2 targeting to LDs and promoting ATGL targeting to LDs in both
339 *CDS2*-deficient cell lines and primary hepatocytes.

340

341 **MBOAT7 and CDS2 regulate cholesterol excretion through the AMPK pathway**

342 Given that knockdown of *Cds2* and/or *Mboat7* increased hepatic cholesterol levels
343 and overexpression of *Mboat7* reduced hepatic cholesterol levels in *Cds2*$^{f/f}$*;AlbCr*e

344 mice, we investigated the mechanism by which CDS2 and MBOAT7 regulate hepatic
345 cholesterol metabolism. Our results showed that knockdown of *Mboat7* reduced the
346 expression levels of genes in the liver X receptor (LXR) pathway, suggesting
347 impaired cholesterol excretion (Figure 5). Heatmap analysis further confirmed the
348 downregulation of genes (*Abcg5* and *Abcg8*) involved in cholesterol excretion (Figure
349 7A). Activation of the AMPK pathway is known to inhibit SREBP and enhance LXR
350 protein levels. AMPK signaling was downregulated in the liver of sh*Mboat7*, sh*Cds2*,
351 or sh*Mboat7* + sh*Cds2* mice, as indicated by heatmap analysis and western blotting
352 (Figure 7A and Figure S3A-B). In contrast, overexpression of *Mboat7* increased
353 p-AMPK and p-ACC levels in *Cds2*$^{f/f}$*;AlbCre* mice, suggesting that AMPK pathway
354 activity was enhanced (Figure 7B and Figure S3C). This was accompanied by reduced
355 nuclear SREBP2 levels and increased expressions of LXR and its target ABCA1 in
356 *Cds2*$^{f/f}$*;AlbCre* mice (Figure 7B). Accordingly, mRNA analysis revealed that
357 downstream targets of LXR (*Abca1*, *Abcg5* and *Abcg8*) were upregulated in the liver
358 of *Mboat7*-overexpressing *Cds2*$^{f/f}$*;AlbCre* mice (Figure 7C).
359 We then investigated whether pharmacological activation of AMPK could reverse
360 the MASLD phenotype in *Cds2*- or *Mboat7*-deficient mice. 8-week-old mice were
361 injected with either AAV-TBG-sh*Cds2* or AAV-TBG-sh*Mboat7* and concurrently fed a
362 NASH-inducing GAN diet for 4 weeks. During the final 2 weeks of this period, mice
363 received intraperitoneal injections of the AMPK agonist A769662 (30 mg/kg, twice
364 daily; Figure 7D). Following A769662 treatment, body weight was reduced in both
365 *Cds2*- and *Mboat7*-deficient mice (Figure S3D). Although plasma triglyceride and
366 cholesterol levels remained unchanged, hepatic levels of triglyceride and cholesterol
367 were significantly decreased (Figure 7E-H). Additionally, A769662 treatment lowered
368 plasma ALT levels, indicating reduced liver inflammation (Figure 7I). H&E and
369 Oil-Red-O staining confirmed a marked reduction in hepatic lipid accumulation in
370 A769662-treated mice compared to vehicle controls (Figure S3E). To assess
371 downstream signaling, we examined the AMPK-LXR axis. A769662 treatment
372 increased protein levels of p-ACC, LXR and ABCA1 in sh*Cds2* and sh*Mboat7* livers
373 (Figure 7J and Figure S3F). Together, these findings suggest that MBOAT7 and CDS2

374 regulate cholesterol excretion through activation of the AMPK-LXR axis.

375

376 **Discussion**

377 Here, we elucidate that spatial localization of MBOAT7 to ER-LD contact
378 sites-orchestrated by CDS2-represents a fundamental cellular adaptation to lipid
379 overload. This redistribution is critical for its role in regulating LD dynamics. At the
380 ER, CDS2 binds to MBOAT7, but in the absence of CDS2, MBOAT7 binds to
381 RAB1A and locates to the ER-LD contacts. There, by sequestering RAB1A,
382 MBOAT7 competitively disrupts the RAB1A-DGAT2 interaction, thereby inhibiting
383 DGAT2-mediated LD growth and promoting lipolysis (Figure 7K).

384 LDs play an essential role in adaptation to fluctuating metabolic states, through
385 controlling their size, subcellular distribution and interaction with other organelles
386 (36). Under lipid overload, cells sequester free fatty acid as triglyceride within the
387 core of LDs to prevent lipotoxicity and oxidative stress. Concurrently, they activate
388 counterregulatory mechanisms to prevent excessive LD accumulation (4).
389 Phospholipid metabolic enzymes, which supply lipids for LD formation, are actively
390 involved in this process. Our study identifies MBOAT7 and CDS2 as key coordinators
391 of LD growth. In MASLD mouse livers, MBOAT7 is more concentrated on LDs
392 compared to normal controls, suggesting a compensatory mechanism to restrain
393 steatosis-driven LD expansion. This represents a protective response in MASLD
394 pathogenesis, whereby the redistribution of an ER protein to ER-LD contacts serves
395 to limit LD growth under lipid overload.

396 ER-LD contact is a critical metabolic hub that maintain organelle function and
397 metabolic homeostasis (8, 12, 37). Although lipid metabolic enzymes are present at
398 these sites, their precise roles are still being defined. Emerging evidence underscores
399 the importance of ER-LD contacts as central platforms for lipid, particularly
400 phospholipid metabolism (38, 39). For instance, LPCAT3, a member of the MBOAT
401 family, localizes at the ER-LD contacts and remodels the acyl-chain composition of
402 phosphatidylethanolamine (PE) to influence LD growth (38). In contrast, MBOAT7
403 regulates LD size independent of its enzymatic activity, highlighting the diverse

404 strategies employed at these contact sites. The broader physiological significance of
405 ER-LD contacts in coordinating lipid metabolism is exemplified In *Cds2* deficient
406 hepatocytes. The compensatory redistribution of MBOAT7 to ER-LD contacts
407 stimulates ATGL-mediated lipolysis, reducing LD size, elevating cytosolic free fatty
408 acids, and promoting cholesterol excretion. Thus, ER-LD contacts function not
409 merely as passive tethers for protein trafficking, but dynamic regulatory nodes that
410 integrate phospholipid remodeling with neutral lipid turnover, ensuring metabolic
411 adaptation and homeostasis.

412 RAB1 is a central player of ER-to-Golgi transport, also plays a central role in
413 recruiting multiple lipid metabolizing enzymes to LDs, thereby fine-tuning LD
414 dynamics and lipid homeostasis (13, 33). Here we found that RAB1A interacts with
415 MBOAT7 and promotes its redistribution to LD surface. This interaction competes
416 DGAT2-mediated LD growth, shifting the metabolic balance toward lipolysis.
417 Importantly, this competitive recruitment only becomes evident under CDS2
418 deficiency, suggesting that RAB1 exhibits a stronger binding affinity for DGAT2 than
419 for MBOAT7. Given that RAB1A and RAB1B share 92% amino acid identity and
420 display functional redundancy (40), our findings consolidate a model in which RAB1
421 serves as a multimodal adaptor that dynamically orchestrate the LD localization of
422 key enzymes involved in both neutral lipid and phospholipid metabolism.

423 In summary, our findings reveal a previously unrecognized axis of inter-organelle
424 communication and metabolic control, orchestrated by MBOAT7, CDS2, and RAB1A
425 that adaptively responds to lipid overload. We provide a new mechanistic link
426 between organelle membrane dynamics and metabolic homeostasis in MASLD
427 pathogenesis.

428

429 **Material and Methods**

430 **Mice**

431 *Cds2*$^{f/f}$ and *Cds2*$^{f/f}$*;AlbCre* mice were generated as described (26). C57BL/6J mice
432 were purchased from GemPharmatech Co., Ltd. For liver-specific gene knockdowns,
433 C57BL/6J mice were injected with AAV-TBG-sh*Con*, AAV-TBG-sh*Mboat7*,

434 AAV-TBG-sh*Cds2* intravenously (i.v) with $3x10^{11}$ genomic copies of AAVs. The
435 target sequence for *Mboat7* is 5'-CCTGTTGGCTTCCTCTTTAAG-3'. The target
436 sequence for *Cds2* is 5'-GTCCGAAGCAAAGCTAGAT-3'. The control sequence is
437 5'-GAAGTCGTGAGAAGTAGAA-3'. For liver-specific overexpression of *Mboat7*,
438 C57BL/6J mice were injected with AAV-TBG-*Con* or AAV-TBG-*Mboat7*
439 intravenously (i.v) with $1x10^{11}$ genomic copies of AAVs. Mice were housed at room
440 temperature (22°C) and fed a standard rodent chow diet (Beijing HFK Bioscience Co.,
441 Ltd #1032). Unless otherwise stated, 8-week-old male mice were used and all mice
442 were fasted for 5-6 hours prior to euthanization. In some experiments, C57BL/6J mice
443 were fed a chow or GAN diet (Research Diets Inc, D09100310) for 26 weeks. All
444 animal experiments were approved by the Institutional Animal Care and Use
445 Committee (IACUC) at the Institute of Genetics and Developmental Biology, Chinese
446 Academy of Sciences (IGDB-CAS).

447 **Cell culture**

448 The *CDS2* knockout HeLa cell line was generated using the CPISPR/Cas9 system
449 according to published literature (41). The target sequence was
450 5'-TATTTACTGAGAATCCGCAA-3'. HepG2 cells (ATCC, HB-8065) and HeLa
451 cells were cultured in DMEM with 10% FBS. In certain experiments, HeLa cells were
452 transfected with siRNAs. The targeting sequence for *RAB1A* is
453 5'-CAGCATGAATCCCGAATAT-3'. The targeting sequence for *CDS2* is
454 5'-GGCCACCTTTGTCAATGTA-3'. Mouse primary hepatocytes were isolated from
455 *Cds2$^{f/f}$* and *Cds2$^{f/f}$;AlbCre* mice and infected with Ad-*EGFP* or Ad-*MBOAT7-EGFP*
456 with MOI=50. All cells were grown at 37°C in a 5% CO_2 incubator.

457 **APEX-based proximity labeling**

458 The cDNA encoding CDS2 was cloned into *pcDNA3APEX2-NES* vector, generating
459 C-terminal fusion protein. Cells expressing the APEX2-CDS2 were incubated with
460 500μM biotin-phenol for 1 hour at 37ºC, followed by a 1-minute labeling reaction
461 initiated by the addition of 1 mM H_2O_2. The reaction was promptly quenched with a
462 TBS solution (Thermo #28376), and the cells were harvested using RIPA buffer.
463 Following cell lysis, biotinylated proteins were affinity-purified using

464 streptavidin-coated beads. After washing, the captured proteins were subjected to
465 on-bead tryptic digestion, and the resulting peptides were analyzed by liquid
466 chromatography-tandem mass spectrometry (LC-MS/MS). Specific proximal
467 interactors were distinguished from background by comparison with cells expressing
468 APEX2 alone.

469 **Plasmids**

470 Human *MBOAT7* cDNA was cloned into the *pcDNA3.1-EGFP* and *pCMV-C-mCherry*
471 vectors. Human *CDS2* cDNA was cloned into the *pCMV-Tag2b* and *pCS2-HA* vectors.
472 Human *RAB1A*, *DGAT2* and *GPAT4* cDNAs were cloned into both the *pEGFP-N1*
473 and *pCMV-Tag2b* vectors.

474 **MBOAT7 activity assay**

475 The activity of MBOAT7 was measured as described with minor modifications (28).
476 Briefly, 100 μg of protein from liver was incubated in 200 μl of medium (10 mM
477 Tris/HCl, pH 7.5, 150 mM NaCl, 1 mM EDTA) with 50 μM lysophosphatidylinositol
478 (LPI), 25 μM arachidonoyl-CoA (20:4-CoA), and 5 μM (0.2 μCi) radiolabeled
479 arachidonoyl[1-14C]CoA. The reaction was incubated for 15-30 minutes at 37 ºC and
480 then stopped by adding 1 mL of chloroform:methanol (2:1, vol/vol) and 0.4 mL of 2%
481 orthophosphoric acid. After centrifugation (3,500 g, 15 min, 4 ºC), the lower organic
482 phase, containing the lipids, was collected and dried under a gentle nitrogen stream.
483 Lipids were reconstituted in chloroform. Total lipids were extracted using the Bligh
484 and Dyer method and separated by one-dimensional TLC on silica gel 60 plates using
485 chloroform/methyl acetate:1-propanol:methanol:0.25% KCl (25:25:25:10:9, vol/vol).
486 The radioactivity in the separated bands were quantified using a Typhoon FLA 9000
487 (GE Healthcare Japan). The corresponding areas of radiolabeled phospholipids on
488 TLC plates were cut out, and the radiolabeled products were measured by liquid
489 scintillation counting.

490 **Lipid analysis**

491 Lipids were extracted based on the chloroform/methanol (2:1, v/v) lipid extraction
492 method (3). In brief, 50 mg of liver tissue were extracted with 6 mL of
493 chloroform/methanol (2:1, v/v), then vortexed and refrigerated overnight. 3 mL of

494 0.043% magnesium chloride was then added to separate the aqueous phase from the
495 chloroform phase which contains the lipids. After separation of the two phases, the
496 upper water/methanol phase was removed. A 0.5-mL aliquot of the bottom phase was
497 combined with 1 mL of 0.5% Triton X-100 in chloroform and dried. Triglyceride and
498 total cholesterol levels were measured using commercially available kits (BioSino,
499 Beijing, China). Plasma free fatty acids (FFA) were measured using commercially
500 available kits (Sigma-Alrich, MAK044).

501 **Immunoprecipitation**

502 Cells were transfected with the indicated plasmids using Lipofectamine 3000
503 (ThermoFisher, L3000001). Proteins were extracted using RIPA lysis buffer,
504 containing100 mM Tris Base, 1% deoxycholate, 0.1% SDS, 5 mM EDTA, 1%
505 Triton-X-100, 150 mM NaCl, pH 8.0), supplemented with 100 mM PMSF, protease
506 inhibitor cocktail (Roche, P8340) and 100 mM sodium vanadate. Lysates were
507 incubated on ice for 15 min, then centrifuged at 12,000 rpm for 15 minutes at 4 °C.
508 Supernatants were incubated overnight at 4 °C with anti-Flag M2 affinity gel
509 (Sigma-Aldrich, A2220) or anti-GPF agarose beads (Lablead Biotech Co., Ltd). After
510 four washes with lysis buffer, beads were denatured in 2X SDS sample buffer for 10
511 min at 100 °C for western blotting. For the pulldown assay, MBOAT7-His was pulled
512 down using Ni-NTA agarose beads (Qiagen, 30210), then washed three times with
513 PBS + PMSF + 1% Triton buffer. 10 μg of *Flag-CDS2* was expressed in 293T cells,
514 immunoprecipitated using anti-Flag M2 affinity gel, and eluted with 3X Flag peptide.
515 The eluted Flag-CDS2 (1.5 mL) was then incubated with the Ni-NTA agarose-bound
516 MBOAT7-His for 2 hours. The immunoprecipitate was washed six times with PBS +
517 PMSF + 1% Triton buffer and denatured with 2X SDS sample buffer for 10 min
518 before western blotting.

519 **Confocal imaging**

520 The images were acquired using a LSM 980 with Airyscan 2 (Zeiss) or a confocal
521 microscope (Leica SP8). Images were analyzed by Image J.

522 **Subcellular fractionation**

523 Subcellular fractionation of liver tissue was performed as described (42).

524 **Antibodies**

525 Rabbit antibodies against CDS2 (1:500, 13175-1-AP), SREBP2 (1:1000,
526 28212-1-AP), LDLR (1:1000, 10785-1-AP), SR-B1 (1:1000, 21277-1-AP) and
527 MBOAT7 (1:100, 83546-3-RR) were purchased from Proteintech. Rabbit antibody
528 against MBOAT7 (1:1000, AV49811) was purchased from Sigma-Aldrich. Mouse
529 antibody against Flag (1:1000, F1804) was purchased from Sigma-Aldrich. Rabbit
530 antibody against Flag (1:2500, PM020) was purchased from MBL. Rabbit antibody
531 against ATGL (1:1000, 2138) was purchased from Cell Signaling Technology. Mouse
532 antibody against LXR (1:1000, ab41902) was purchased from Abcam. Rabbit
533 antibodies against DGAT2 (1:1000, ab237613) and HMGCR (1:1000, ab174830)
534 were purchased from Abcam.

535 **Statistics**

536 Results with error bars are mean±SEM. Comparisons between 2 groups were
537 performed using the two-tailed Student's t-test. ANOVA was used for comparisons
538 between more than 2 groups.

539 **Acknowledgments**

540 We thank Xixian Li from the Center for Biological Imaging at the Institute of
541 Biophysics, CAS, for analyzing images. This work was supported by grants
542 2024YFA1306101, 2023YFA1800500 from National Key R&D Program of China
543 and 92354301, 32230044, 32371230 and 32321004 from the National Natural Science
544 Foundation of China, and BJ-2024-235 from National High Level Hospital Clinical
545 Research Funding.

546 Figure 3A, Figure 6C and Figure 7K were created with BioRender
547 (*https://BioRender.com/ k88h902*, *https://BioRender.com/s73x778, and*
548 *https://BioRender.com/e57c295*).

549 **Declaration of Interests**

550 The authors have declared that no conflict of interest exists.

551 **Author Contributions**

552 J Xu and X Huang designed the experiments. J Xu, J Zhang, W Wang and H Su
553 performed the experiments. J Xu, J Zhang, S Chen and M Ding analyzed the data. J

554 Xu and X Huang wrote the manuscript.

555

556 **References**

557 1. L. Xiang *et al.*, A multi-omic landscape of steatosis-to-NASH progression. *Life Metab* **1**,
558 242-257 (2022).
559 2. T. C. Walther, J. Chung, R. V. Farese, Jr., Lipid Droplet Biogenesis. *Annu Rev Cell Dev Biol* **33**,
560 491-510 (2017).
561 3. E. Scorletti, R. M. Carr, A new perspective on NAFLD: Focusing on lipid droplets. *J Hepatol* **76**,
562 934-945 (2022).
563 4. J. L. Dempsey, G. N. Ioannou, R. M. Carr, Mechanisms of Lipid Droplet Accumulation in
564 Steatotic Liver Diseases. *Semin Liver Dis* **43**, 367-382 (2023).
565 5. N. L. Gluchowski, M. Becuwe, T. C. Walther, R. V. Farese, Jr., Lipid droplets and liver disease:
566 from basic biology to clinical implications. *Nat Rev Gastroenterol Hepatol* **14**, 343-355 (2017).
567 6. M. B. Schott *et al.*, Lipid droplet size directs lipolysis and lipophagy catabolism in hepatocytes.
568 *J Cell Biol* **218**, 3320-3335 (2019).
569 7. G. F. Grabner, H. Xie, M. Schweiger, R. Zechner, Lipolysis: cellular mechanisms for lipid
570 mobilization from fat stores. *Nat Metab* **3**, 1445-1465 (2021).
571 8. K. Qian *et al.*, CLSTN3beta enforces adipocyte multilocularity to facilitate lipid utilization.
572 *Nature* **613**, 160-168 (2023).
573 9. G. E. Miner *et al.*, PLIN5 interacts with FATP4 at membrane contact sites to promote lipid
574 droplet-to-mitochondria fatty acid transport. *Dev Cell* **58**, 1250-1265 e1256 (2023).
575 10. A. Kumar, S. Yadav, V. Choudhary, The evolving landscape of ER-LD contact sites. *Front Cell*
576 *Dev Biol* **12**, 1483902 (2024).
577 11. M. J. Olarte *et al.*, Determinants of Endoplasmic Reticulum-to-Lipid Droplet Protein Targeting.
578 *Dev Cell* **54**, 471-487 (2020).
579 12. D. Li *et al.*, The ER-Localized Protein DFCP1 Modulates ER-Lipid Droplet Contact Formation.
580 *Cell Rep* **27**, 343-358 e345 (2019).
581 13. J. Song *et al.*, Identification of two pathways mediating protein targeting from ER to lipid
582 droplets. *Nat Cell Biol* **24**, 1364-1377 (2022).
583 14. A. Caddeo, R. Spagnuolo, S. Maurotti, MBOAT7 in liver and extrahepatic diseases. *Liver Int* **43**,
584 2351-2364 (2023).
585 15. V. R. Thangapandi *et al.*, Loss of hepatic Mboat7 leads to liver fibrosis. *Gut* **70**, 940-950
586 (2021).
587 16. V. Varadharajan, W. J. Massey, J. M. Brown, Membrane-bound O-acyltransferase 7
588 (MBOAT7)-driven phosphatidylinositol remodeling in advanced liver disease. *J Lipid Res* **63**,
589 100234 (2022).
590 17. J. Alharthi *et al.*, A metabolic associated fatty liver disease risk variant in MBOAT7 regulates
591 toll like receptor induced outcomes. *Nat Commun* **13**, 7430 (2022).
592 18. M. Xia, P. Chandrasekaran, S. Rong, X. Fu, M. A. Mitsche, Hepatic deletion of Mboat7 (LPIAT1)
593 causes activation of SREBP-1c and fatty liver. *J Lipid Res* **62**, 100031 (2021).
594 19. Y. Liu, W. Wang, G. Shui, X. Huang, CDP-diacylglycerol synthetase coordinates cell growth and
595 fat storage through phosphatidylinositol metabolism and the insulin pathway. *PLoS Genet* **10**,
596 e1004172 (2014).

597 20. N. J. Blunsom, S. Cockcroft, CDP-Diacylglycerol Synthases (CDS): Gateway to
598 Phosphatidylinositol and Cardiolipin Synthesis. *Front Cell Dev Biol* **8**, 63 (2020).
599 21. K. D'Souza, Y. J. Kim, T. Balla, R. M. Epand, Distinct properties of the two isoforms of
600 CDP-diacylglycerol synthase. *Biochemistry* **53**, 7358-7367 (2014).
601 22. M. P. Moore *et al.*, Low MBOAT7 expression, a genetic risk for MASH, promotes a profibrotic
602 pathway involving hepatocyte TAZ upregulation. *Hepatology* **81**, 576-590 (2024).
603 23. Y. Tanaka *et al.*, LPIAT1/MBOAT7 depletion increases triglyceride synthesis fueled by high
604 phosphatidylinositol turnover. *Gut* **70**, 180-193 (2021).
605 24. Y. Xu *et al.*, CDP-DAG synthase 1 and 2 regulate lipid droplet growth through distinct
606 mechanisms. *J Biol Chem* **294**, 16740-16755 (2019).
607 25. Y. Qi *et al.*, CDP-diacylglycerol synthases regulate the growth of lipid droplets and adipocyte
608 development. *J Lipid Res* **57**, 767-780 (2016).
609 26. J. Xu *et al.*, Hepatic CDP-diacylglycerol synthase 2 deficiency causes mitochondrial
610 dysfunction and promotes rapid progression of NASH and fibrosis. *Sci Bull (Beijing)* **67**,
611 299-314 (2022).
612 27. J. A. Olzmann, P. Carvalho, Dynamics and functions of lipid droplets. *Nat Rev Mol Cell Biol* **20**,
613 137-155 (2019).
614 28. K. Wang *et al.*, The structure of phosphatidylinositol remodeling MBOAT7 reveals its catalytic
615 mechanism and enables inhibitor identification. *Nat Commun* **14**, 3533 (2023).
616 29. R. Dhiman, S. Caesar, A. R. Thiam, B. Schrul, Mechanisms of protein targeting to lipid droplets:
617 A unified cell biological and biophysical perspective. *Semin Cell Dev Biol* **108**, 4-13 (2020).
618 30. C. I. Pataki *et al.*, Proteomic analysis of monolayer-integrated proteins on lipid droplets
619 identifies amphipathic interfacial alpha-helical membrane anchors. *Proc Natl Acad Sci U S A*
620 **115**, E8172-E8180 (2018).
621 31. K. Bersuker *et al.*, A Proximity Labeling Strategy Provides Insights into the Composition and
622 Dynamics of Lipid Droplet Proteomes. *Dev Cell* **44**, 97-112 e117 (2018).
623 32. N. Mejhert *et al.*, Partitioning of MLX-Family Transcription Factors to Lipid Droplets Regulates
624 Metabolic Gene Expression. *Mol Cell* **77**, 1251-1264 e1259 (2020).
625 33. Y. Malis *et al.*, Rab1b facilitates lipid droplet growth by ER-to-lipid droplet targeting of DGAT2.
626 *Sci Adv* **10**, eade7753 (2024).
627 34. F. Wilfling *et al.*, Triacylglycerol synthesis enzymes mediate lipid droplet growth by
628 relocalizing from the ER to lipid droplets. *Dev Cell* **24**, 384-399 (2013).
629 35. M. Meroni *et al.*, Mboat7 down-regulation by hyper-insulinemia induces fat accumulation in
630 hepatocytes. *EBioMedicine* **52**, 102658 (2020).
631 36. R. W. Klemm, P. Carvalho, Lipid Droplets Big and Small: Basic Mechanisms That Make Them
632 All. *Annu Rev Cell Dev Biol* **40**, 143-168 (2024).
633 37. D. Xu *et al.*, Rab18 promotes lipid droplet (LD) growth by tethering the ER to LDs through
634 SNARE and NRZ interactions. *J Cell Biol* **217**, 975-995 (2018).
635 38. M. J. Tol *et al.*, Dietary control of peripheral adipose storage capacity through membrane lipid
636 remodelling. *Nat Metab* **7**, 1424-1442 (2025).
637 39. Q. Li, X. Zhou, X. Zhang, C. Zhang, S. O. Zhang, Nuclear receptor signaling regulates
638 compartmentalized phosphatidylcholine remodeling to facilitate thermosensitive lipid
639 droplet fusion. *Nat Commun* **16**, 3955 (2025).
640 40. X. Z. Yang *et al.*, Rab1 in cell signaling, cancer and other diseases. *Oncogene* **35**, 5699-5704

641 (2016).
642 41. F. A. Ran *et al.*, Genome engineering using the CRISPR-Cas9 system. *Nat Protoc* **8**, 2281-2308
643 (2013).
644 42. Y. Ding *et al.*, Isolating lipid droplets from multiple species. *Nat Protoc* **8**, 43-51 (2013).
645

646 **Figure Legends**

647 **Figure 1. MBOAT7 is localized to the ER-LD contacts in CDS2 KO cells.**
648 (A) MBOAT7 enzymatic activity was measured in *Cds2*$^{f/f}$, *Cds2*$^{f/f}$*;AlbCre* mice, and
649 *Cds2*$^{f/f}$*;AlbCre* mice injected with AAV-TBG-*Cds2*. N=5-6 mice per group. (B) *CDS2*
650 KO and control HeLa cells were transfected with MBOAT7-EGFP and treated with
651 100 μM OA for 12 hours, followed by LD labeling with LipidTOX. (C) Fluorescence
652 colocalization was analyzed along the white line in the main confocal image. (D)
653 *CDS2* KO and control HeLa cells were treated with 100 μM OA for 12 hours and
654 immunostained with anti-MBOAT7 antibody. White arrows indicate nicks on LD
655 surface. (E) Fluorescence colocalization was analyzed along the white line in the main
656 confocal image. (F) A 3D-SIM image reveals that MBOAT7-EGFP enwraps a LD in
657 an OA-treated *CDS2* KO cell. Scale bar: 2 μm. (G) *CDS2* KO and control HeLa cells
658 were transfected with mCherry-SEC61b (an ER marker), then treated with 100 μM
659 OA for 12 hours. LDs were labeled with BODIPY. (H) Fluorescence colocalization
660 was analyzed along the white line in the main confocal image. (I) C56BL/6 mice were
661 fed a chow (control) or GAN (MASLD) diet (40 kcal% fat, 20 kcal% fructose and 2%
662 cholesterol) for 26 weeks. Liver sections were immunostained with anti-MBOAT7
663 antibody. White arrows indicate MBOAT7 enclosing LDs. (J) The number of LDs
664 surrounded by MBOAT7 was quantified by analyzing 1,000 LDs in confocal images.
665 N=9-11 liver sections per group. (K) Top: 3D structure of MBOAT7 in the ER
666 membrane, highlighting its transmembrane (TM) domains. Bottom: The 11 TM
667 domains of MBOAT7 (boxes) and the three regions of the protein expressed as
668 truncations. (L) *CDS2* KO cells transfected with truncated versions of MBOAT7 were
669 treated with 100 μM OA for 12 hours, followed by LD labeling with LipidTOX.
670 Except for (F), scale bars represent 10 μm in main images and 2 μm in enlarged
671 images.

672

673 **Figure 2. MBOAT7 interacts with CDS2.**

674 (A) Co-IP assay showing that Flag-CDS2 precipitates MBOAT7-EGFP. (B) Co-IP
675 assay showing that MBOAT7-EGFP precipitates Flag-CDS2. (C) Co-IP assay
676 demonstrating that endogenous CDS2 precipitates MBOAT7. (D) *In vitro* pull-down
677 assay indicating that Flag-CDS2 directly binds to MBOAT7-His.

678

679 **Figure 3. RAB1A is required for targeting of MBOAT7 to LDs in *CDS2* KO cells.**

680 (A) Schematic of the workflow for identifying MBOAT7-interacting proteins in
681 control and *CDS2* KO cells. (B) Venn diagram illustrating the overlap between the
682 MBOAT7-interacting proteins from (A) and LD proteins from various LD proteomes.
683 (C) Five MBOAT7-interacting proteins identified from the Venn diagram in (B). (D)
684 *CDS2* KO cells were transfected with siNC or siRAB1A, and MBOAT7-EGFP, then
685 treated with 100 μM OA for 12 hours. LDs were labeled with LipidTOX. (E) *RAB1A*
686 mRNA levels in HeLa cells transfected with control siRNA or siRAB1A. (F)
687 Quantification of LDs surrounded by MBOAT7-EGFP in control (siNC) or RAB1A
688 knockdown (siRAB1A) cells. (G) Co-IP assay showing that Flag-RAB1A precipitates
689 MBOAT7-EGFP in *CDS2* KO cells. (H) Co-IP assay showing that Flag-RAB1A
690 precipitates MBOAT7-EGFP in *CDS2* KO cells, and expression of HA-CDS2 in
691 *CDS2* KO cells disrupts the RAB1A/MBOAT7 interaction. (I) 3D structure of
692 MBOAT7/RAB1A docking and the potential binding sites. (J) Co-IP assay showing
693 that Flag-RAB1A precipitates MBOAT7-EGFP, but fails to interact with
694 MBOAT7-BS-mut-EGFP, in which the RAB1A-binding sites are mutated in *CDS2*
695 KO cells. *** $p < 0.001$, **** $p < 0.0001$.

696

697 **Figure 4. MBOAT7 reduces LD size in *CDS2* KO cells by competing with DGAT2**
698 **for targeting to LDs.**

699 (A) Control HeLa or *CDS2* KO cells were transfected with MBOAT7-EGFP or the
700 MBOAT7(N321A, H356A)-EGFP mutant, then treated with 100 μM OA for 12 hours.
701 LDs were labeled by LipidTOX. Scale bar: 10 μm. (B) Quantification of LD sizes

702 from (A). N=200 per group. (C) 293T cells were transfected with GFP-RAB1A and
703 Flag-DGAT2 or Flag control plasmids. Co-IP assay shows that Flag-DGAT2
704 precipitates GFP-RAB1A. (D) 293T cells were transfected with GFP-RAB1A and
705 Flag-GPAT4 or Flag control plasmid. Co-IP assay shows that Flag-GPAT4 precipitates
706 GFP-RAB1A. (E) *CDS2* KO cells were transfected with GFP-RAB1A and
707 Flag-GPAT4 with or without MBOAT7-EGFP. Co-IP shows that Flag-GPAT4
708 precipitates GFP-RAB1A. (F) *CDS2* KO cells were transfected with GFP-RAB1A
709 and Flag-DAGT2 with or without MBOAT7-EGFP or MBOAT7-BS-mut-EGFP.
710 Co-IP shows that Flag-DGAT2 precipitates GFP-RAB1A. (G) *CDS2* KO cells were
711 transfected with Flag-DGAT2 and GFP-RAB1A with siRNA control (siCon) or
712 siMBOAT7. Co-IP assay shows that Flag-DGAT2 precipitates GFP-RAB1A. (H)
713 Confocal images showing that EGFP-DGAT2 targets to LDs in *CDS2* KO cells.
714 MBOAT7-mCherry expression blocks LD targeting of DGAT2. Scale bar: 10 μm in
715 main images and 2 μm in enlarged images. (I) Co-IP assay showing that Flag-DGAT2
716 precipitates GFP-RAB1A in *CDS2* KO cells treated with or without OA. (J) Co-IP
717 assay showing that Flag-MBOAT7 precipitates GFP-RAB1A in *CDS2* KO cells
718 treated with or without OA. **** $p < 0.0001$.
719
720 **Figure 5. MBOAT7 and CDS2 coordinately regulate hepatic lipid metabolism.**
721 (A-E) Procedure for liver-specific knockdown of *Mboat7* and/or *Cds2* in mice. Mice
722 were injected with AAV-TBG-shCon, AAV-TBG-sh*Mboat7*, AAV-TBG-sh*Cds2*, or
723 AAV-TBG-sh*Mboat7* + AAV-TBG-sh*Cds2* and fed a chow diet for 4 weeks before
724 analysis (A). Plasma triglyceride (B) and cholesterol (C), as well as hepatic
725 triglyceride (D) and cholesterol (E) levels were measured in the mice in (A). N=6-7
726 mice per group. (F) H&E staining of liver sections from mice in (A). Scale bar
727 represents 50 μm in main images and 10 μm in enlarged images. (G) Hepatic steatosis
728 score based on liver sections of mice in (A). N=6-7 mice per group. (H) RNAseq was
729 performed on liver samples from the mice in A. The numbers of genes up- or
730 down-regulated in sh*Mboat7* vs sh*Con*, sh*Cds2* vs sh*Con* and sh*Mboat7* + sh*Cds2* vs
731 sh*Con* are shown. (I) KEGG analysis results showing the pathways related to the 301

732 common downregulated genes in (A). (J) KEGG analysis results showing the
733 pathways related to the 266 common upregulated genes in (A). (K) qRT-PCR analysis
734 of the mRNA levels of genes that regulate cholesterol and fatty acid metabolism in the
735 liver. N=5-8 mice per group. (L) Western blot analysis of liver lysates. N=3 mice per
736 group. (M) Quantification of protein levels in (D). * $p < 0.05$, ** $p < 0.01$, *** $p <$
737 0.001, **** $p < 0.0001$.
738
739 **Figure 6. MBOAT7 regulates LD size and lipolysis.**
740 (A) Schematic showing the procedure for hepatic overexpression of MBOAT7 in the
741 liver of mice with and without hepatic depletion of *Cds2*. *Cds2*$^{f/f}$ and *Cds2*$^{f/f}$*;AlbCre*
742 mice were injected with AAV-TBG-Con or AAV-TBG-*Mboat7* and fed a chow diet for
743 4 weeks before analysis. (B) Western blot analysis of LD, ER and cytosol fractions
744 from the liver of *Cds2*$^{f/f}$*;AlbCre* mice that are injected with AAV-TBG-Con or
745 AAV-TBG-*Mboat7*. (C) Primary hepatocytes from *Cds2*$^{f/f}$ and *Cds2*$^{f/f}$*;AlbCre* mice
746 were infected with Ad-EGFP or Ad-MBOAT7-EGFP, then treated with 10 μM ISO or
747 DMSO (control) for the indicated times. Free fatty acids in the medium were analyzed.
748 (D and E) Plasma triglyceride (D) and cholesterol (E) levels were analyzed in the
749 mice from (B). (F and G) Hepatic triglyceride (F) and cholesterol (G) levels were
750 analyzed in the mice from (A). N=7-8 mice per group. (H) H&E staining of liver
751 sections from *Cds2*$^{f/f}$ and *Cds2*$^{f/f}$*;AlbCre* mice. Scale bar represents 50 μm in main
752 images and 10 μm in enlarged images. (I) Primary hepatocytes isolated from *Cds2*$^{f/f}$
753 and *Cds2*$^{f/f}$*;AlbCre* mice were infected with Ad-EGFP or Ad-MBOAT7-EGFP and
754 treated with 100 μM OA for 12 hours. LDs were stained with LipdTOX before
755 confocal imaging. Scale bar represents 10 μm in main images and 2 μm in enlarged
756 images. (J) Quantification of LD sizes in (I). * $p < 0.05$, ** $p < 0.01$, *** $p < 0.001$,
757 **** $p < 0.0001$.
758
759 **Figure 7. MBOAT7 and CDS2 regulate cholesterol metabolism through the**
760 **AMPK pathway.**
761 (A) Heatmap analysis shows alterations of expression levels of genes involved in

762 cholesterol metabolism and the AMPK pathway in the liver of 8-week-old mice
763 injected with AAV-TBG-sh*Con*, AAV-TBG-sh*Mboat7*, AAV-TBG-sh*Cds2*, and
764 AAV-TBG-sh*Mboat7* + AAV-TBG-sh*Cds2*. (B) Western blot of *Cds2*$^{f/f}$ and
765 *Cds2*$^{f/f}$*;AlbCre* mice injected with AAV-TBG-Con or AAV-TBG-*Mboat7*, and fed a
766 chow diet for 4 weeks before analysis. (C) qRT-PCR analysis of genes involved in
767 cholesterol and fatty acid metabolism. (D) Schematic showing the procedure for
768 sh*Cds2* and sh*Mboat7* mice with or without A769662 treatment. 8-week-old
769 C57BL6/J mice were injected with either AAV-TBG-sh*Cds2* or AAV-TBG-sh*Mboat7*
770 and concurrently fed a NASH-inducing GAN diet for 4 weeks. During the final 2
771 weeks of this period, mice received intraperitoneal injections of the AMPK agonist
772 A769662 (30 mg/kg, twice daily). (E-H) Plasma triglyceride (E) and cholesterol (F),
773 hepatic triglyceride (G) and cholesterol (H), plasma ALT levels (I) were shown. (J)
774 Protein levels of key components in the LXR signaling pathway. (K) A model
775 illustrating how MBOAT7 and CDS2 regulate LD dynamics and cholesterol
776 metabolism in hepatocytes. CDS2 and MBOAT7 physically interact in the ER
777 membrane and both regulate PI biosynthesis. MBOAT7 catalyzes the generation of
778 PI-AA, which inhibits CDS2 activity. In the absence of CDS2, MBOAT7 relocates to
779 the ER-LD contacts via binding to RAB1. CDS2 deficiency causes increased LD size
780 accompanied by increased recruitment of DGAT2 to LDs, whereas overexpression of
781 MBOAT7 in CDS2-deficient conditions reduces DGAT2 targeting to LDs, increases
782 ATGL recruitment to the LD surface, and reduces LD size. The increased lipolysis
783 induced by MBOAT7 expression activates AMPK, enhancing LXR protein levels and
784 expression of its downstream target genes, thus stimulating cholesterol metabolism. *
785 $p < 0.05$, ** $p < 0.01$, *** $p < 0.001$, **** $p < 0.0001$,
786
787 **Figure S1. APEX-based proximity labeling**
788 (A) APEX-base proximity labeling utilizes an engineered ascorbate peroxidase
789 (APEX2). Upon the addition of hydrogen peroxide, it catalyzes the conversion of
790 bio-phenol into highly reactive, short-lived biotin-phenoxyl radicals, which covalently
791 tag endogenous proteins within a nanometer-scale radius. (B) The proximal partners

792 of APEX2-CDS2.

793

794 **Figure S2. MBOAT7 and CDS2 coordinate hepatic cholesterol and fatty acid**
795 **metabolism.**

796 (A-B) HeLa (A) and CDS2 KO (B) cells were transfected with MBOAT7-EGFP and
797 mCherry-SEC61B for 24 hours. Confocal images are shown. (C) CDS2 KO and
798 control HeLa cells were transfected with mScarlet-PLIN1 and MBOAT7-EGFP and
799 treated with 100 μM OA for 12 hours. Colocalization between mScarlet-PLIN1 and
800 MBOAT7-EGFP is shown. (D) HepG2 cells were transfected with MBOAT7-EGFP
801 and siCDS2 or control siRNA (NC), then treated with 100 μM OA for 12 hours. LDs
802 were stained by LipidTOX. (E) A co-IP assay shows that Flag-GPAT4 precipitates
803 GFP-RAB1A in HeLa cells treated with or without OA. Scale bars represent 10 μm in
804 main images and 2 μm in enlarged images.

805

806 **Figure S3. MBOAT7 and CDS2 regulate cholesterol metabolism through the**
807 **AMPK pathway.**

808 (A) Western blot analysis of liver lysates from 8-week-old mice injected with
809 AAV-TBG-sh*Con*, AAV-TBG-sh*Mboat7*, AAV-TBG-sh*Cds2*, and
810 AAV-TBG-sh*Mboat7* + AAV-TBG-sh*Cds2*. (B) Quantifications of the western blot in
811 (A). (C) Quantifications of proteins from Figure7B. (D) Body weight of sh*Cds2* and
812 sh*Mboat7* mice with or without A769662 treatment. (E) Representative H&E and
813 Oil-Red-O staining for liver sections from the indicated groups in Figure7D. (F)
814 Quantifications of proteins from Figure7J. * $p < 0.05$, ** $p < 0.01$, *** $p < 0.001$,
815 **** $p < 0.0001$, # $p<0.05$, ## $p<0.01$.

A

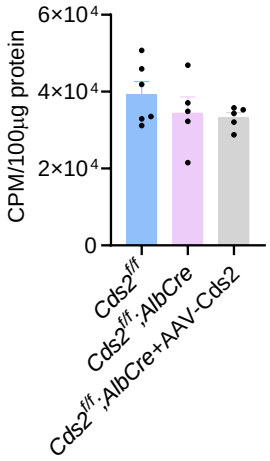

B

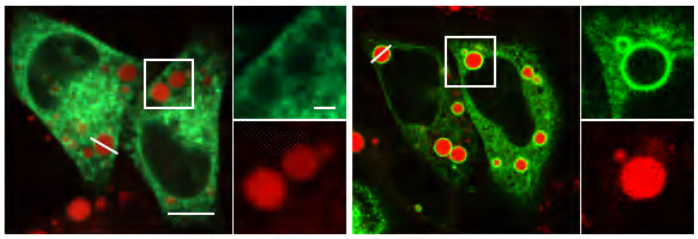

F

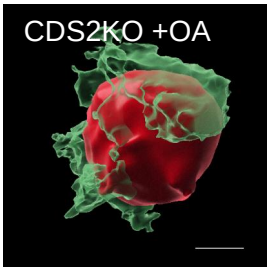

C

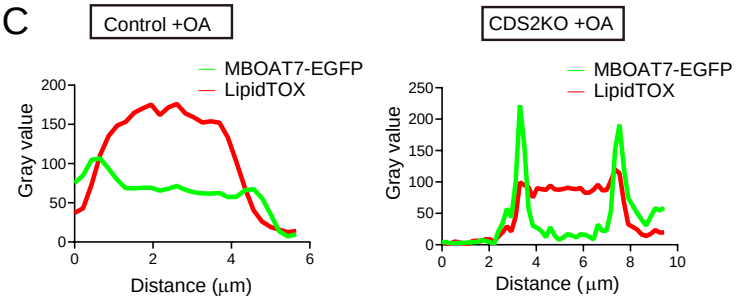

D

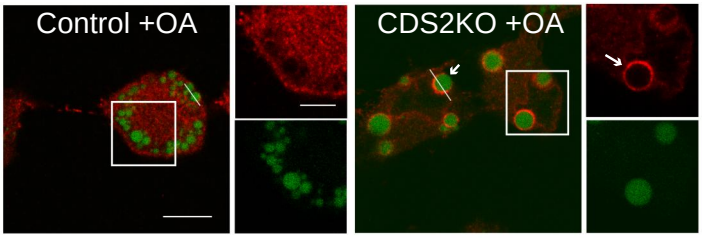

E

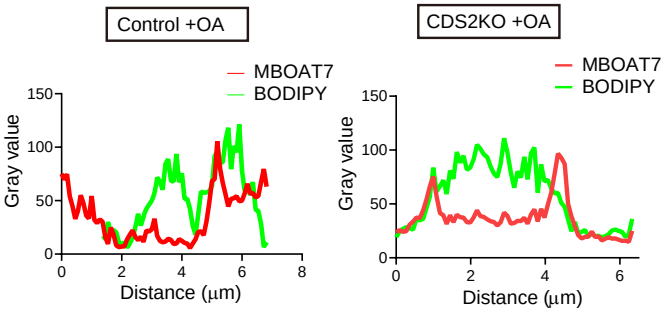

G

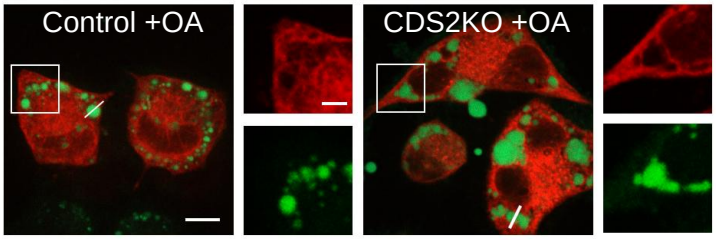

I

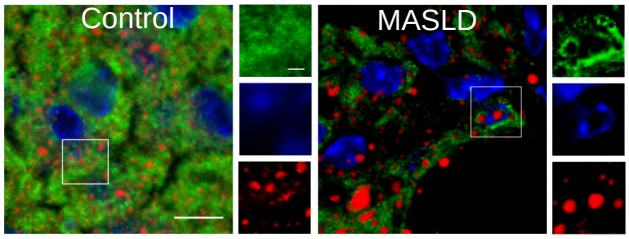

H

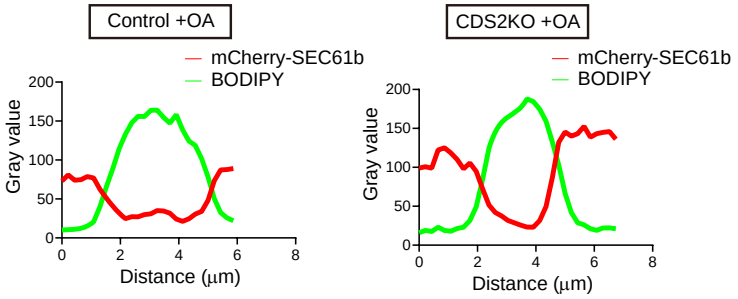

J

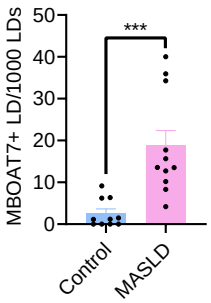

K

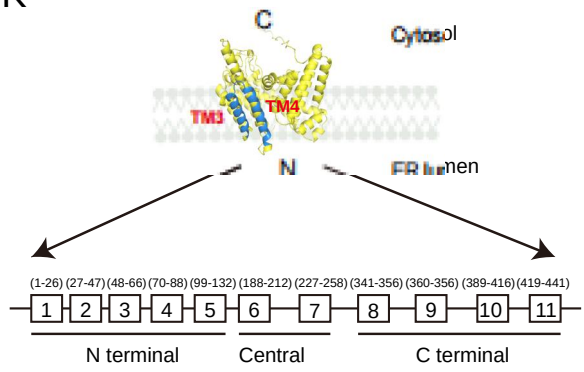

L

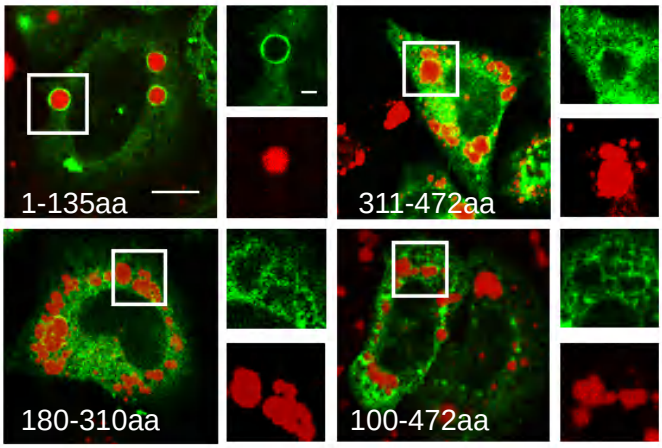

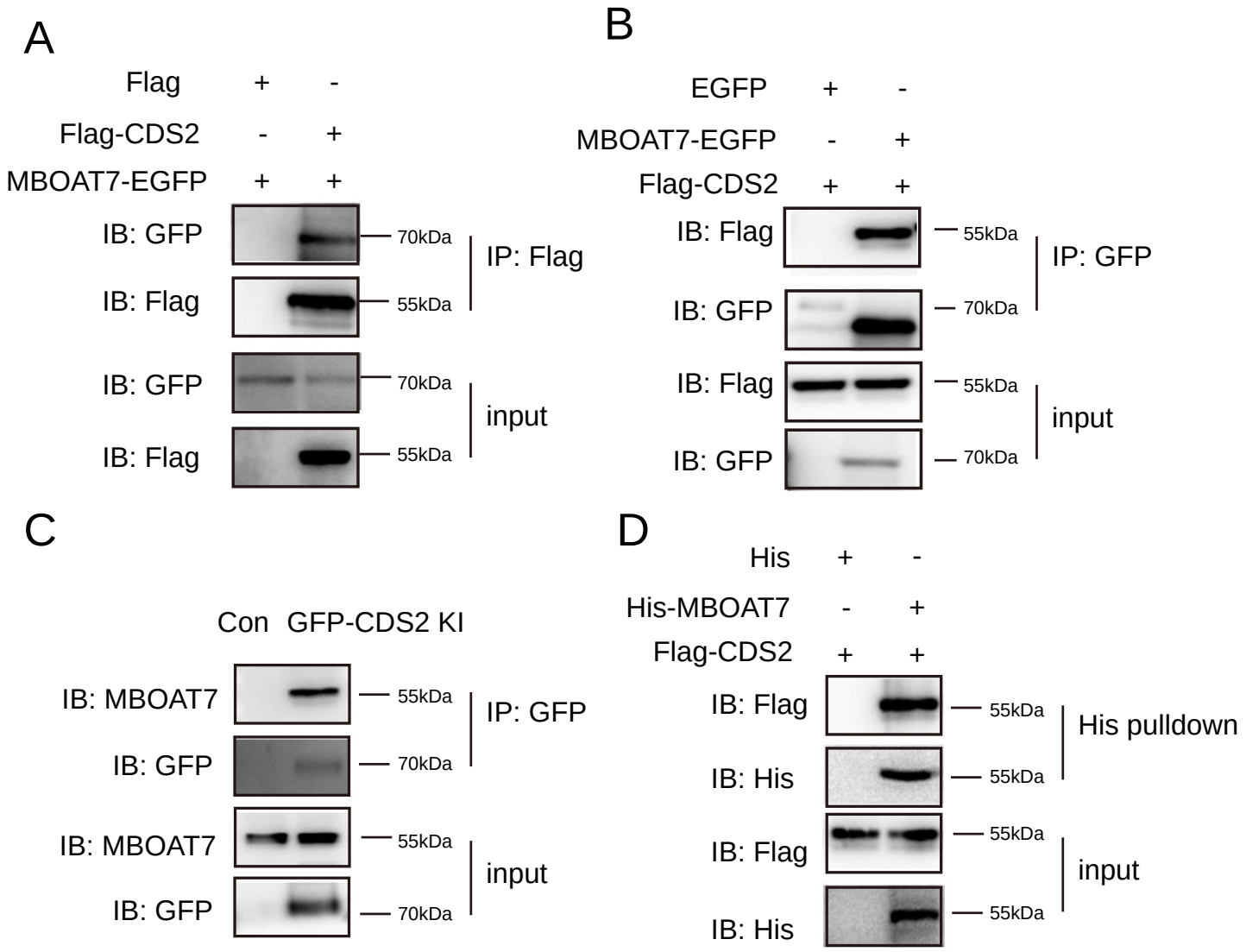
A
Flag + -
Flag-CDS2 - +
MBOAT7-EGFP + +
IB: GFP
IB: Flag
IB: GFP
IB: Flag
70kDa
55kDa
70kDa
55kDa
IP: Flag
input
B
EGFP + -
MBOAT7-EGFP - +
Flag-CDS2 + +
IB: Flag
IB: GFP
IB: Flag
IB: GFP
55kDa
70kDa
55kDa
70kDa
IP: GFP
input
C
Con GFP-CDS2 KI
IB: MBOAT7
IB: GFP
IB: MBOAT7
IB: GFP
55kDa
70kDa
55kDa
70kDa
IP: GFP
input
D
His + -
His-MBOAT7 - +
Flag-CDS2 + +
IB: Flag
IB: His
IB: Flag
IB: His
55kDa
55kDa
55kDa
55kDa
His pulldown
input

A

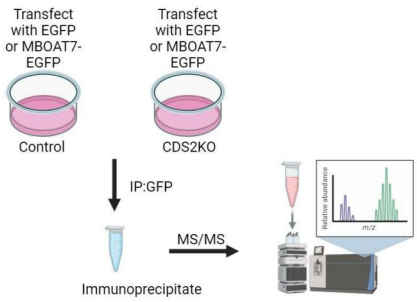

B

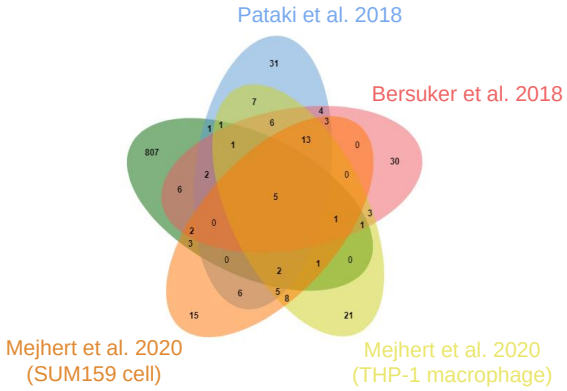

C

Protein	Fold change
RAB7A	10.4
RAB1A	7.2
RAB18	6.2
RAB14	4.8
CYB5R3	4

D

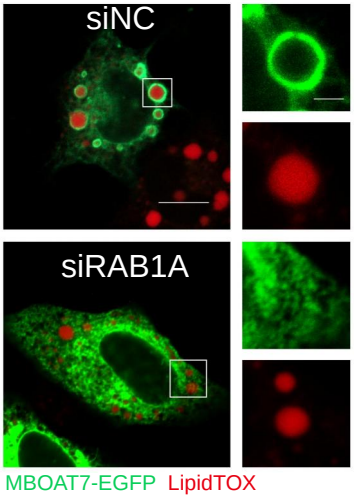

E

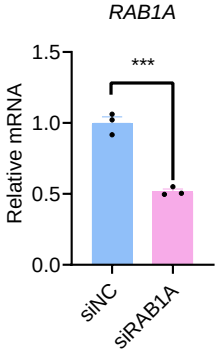

F

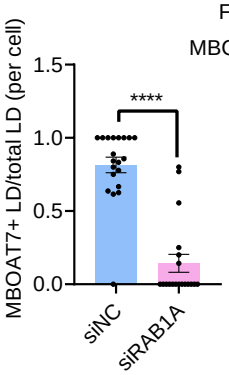

G

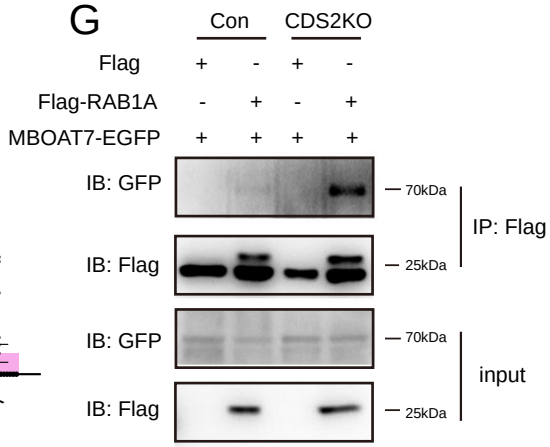

H

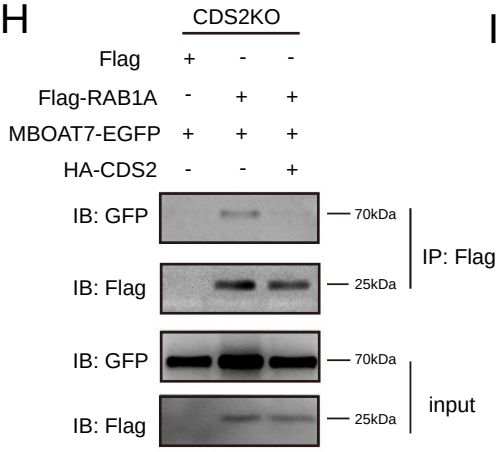

I

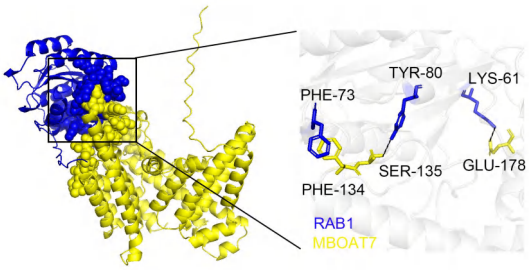

J

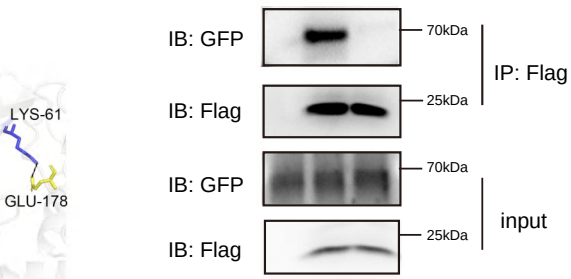

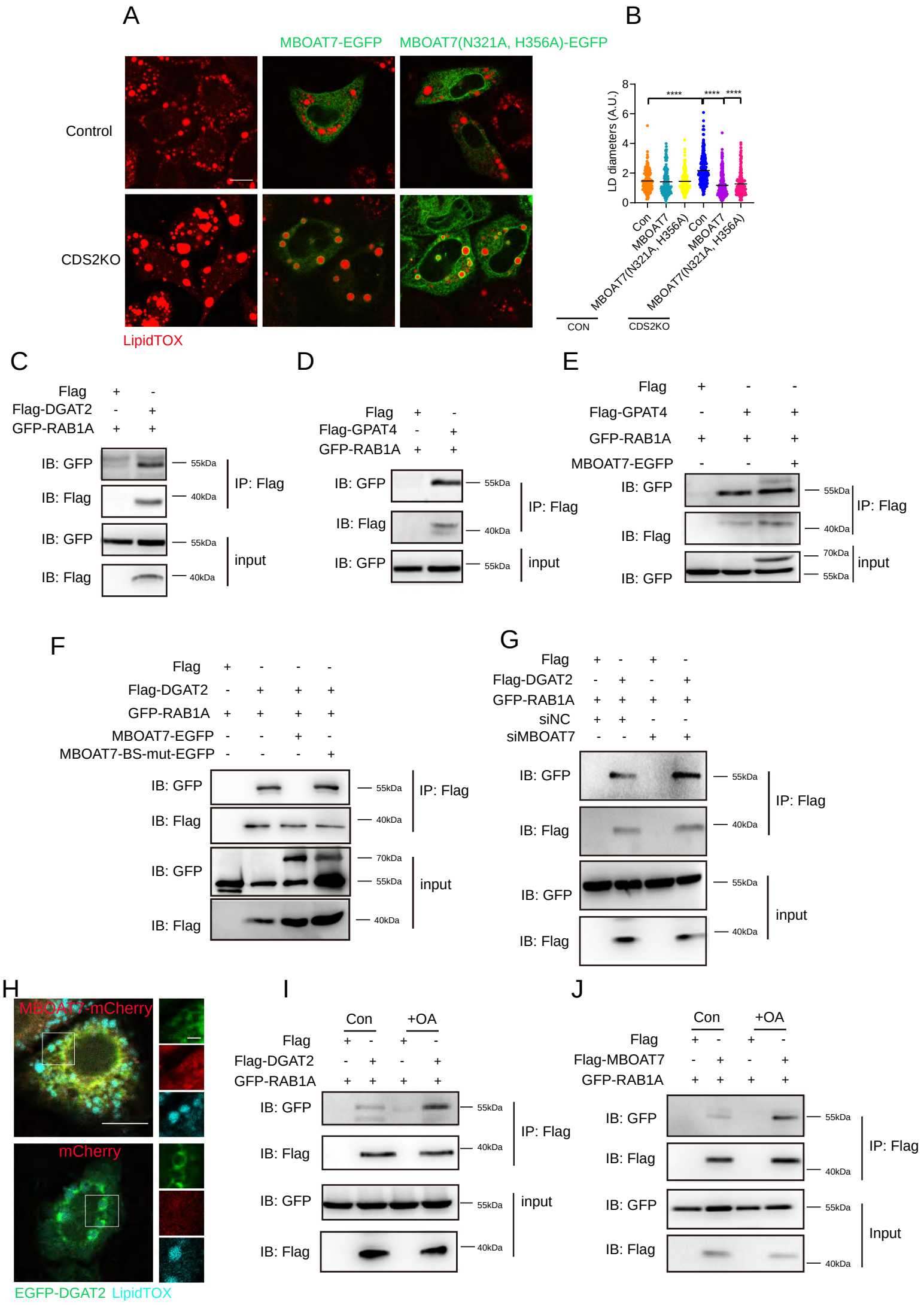
A
MBOAT7-EGFP
MBOAT7(N321A, H356A)-EGFP
Control
CDS2KO
LipidTOX
B
LD diameters (A.U.)
Con
MBOAT7
MBOAT7(N321A, H356A)
CON
CDS2KO
C
Flag
Flag-DGAT2
GFP-RAB1A
IB: GFP
IB: Flag
IP: Flag
input
55kDa
40kDa
D
Flag-GPAT4
E
MBOAT7-EGFP
70kDa
F
MBOAT7-BS-mut-EGFP
G
siNC
siMBOAT7
H
MBOAT7-mCherry
mCherry
EGFP-DGAT2
LipidTOX
I
Con
+OA
J
Flag-MBOAT7
Input

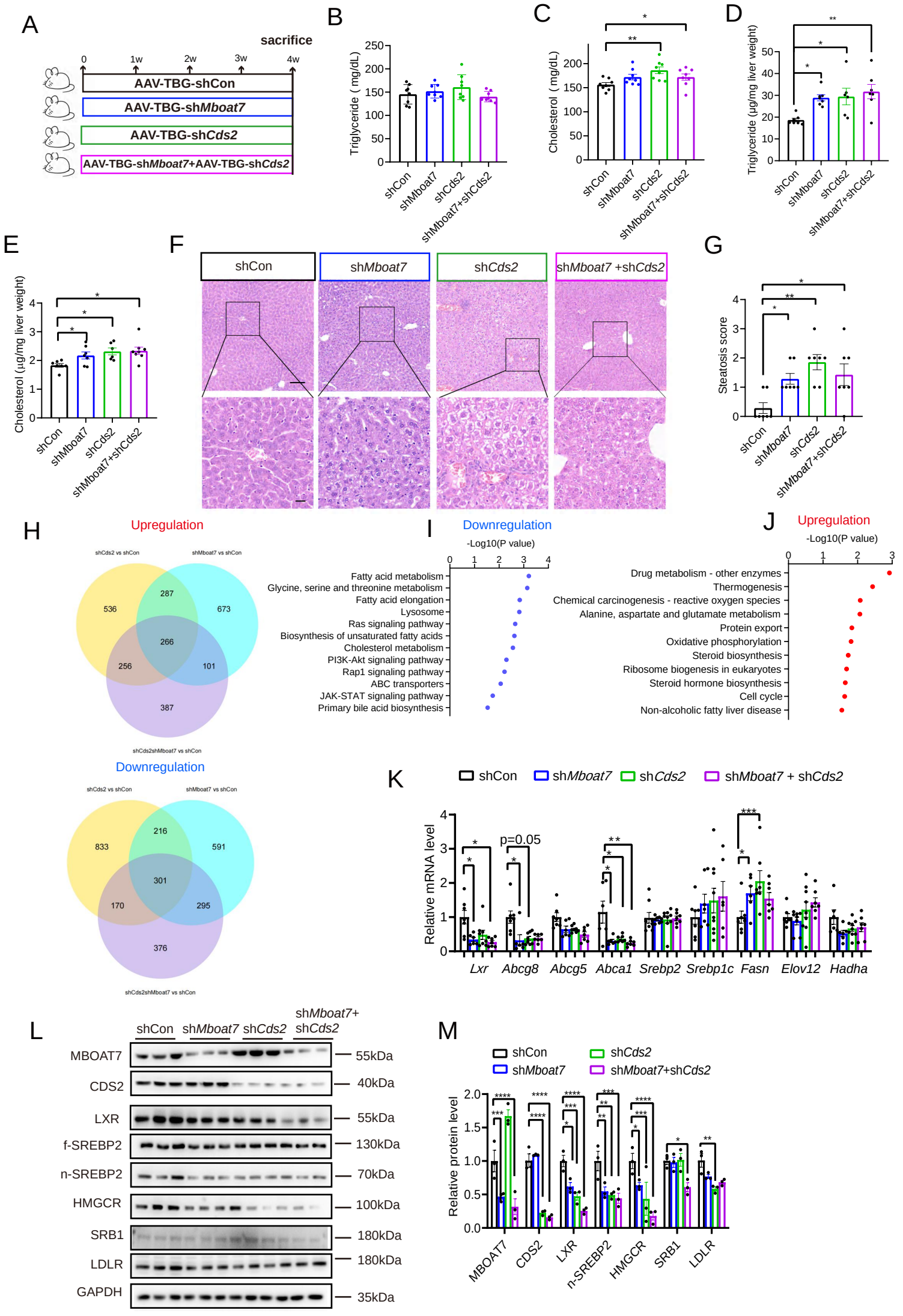
A
sacrifice
0
1w
2w
3w
4w
AAV-TBG-shCon
AAV-TBG-shMboat7
AAV-TBG-shCds2
AAV-TBG-shMboat7+AAV-TBG-shCds2
B
Triglyceride (mg/dL)
C
Cholesterol (mg/dL)
D
Triglyceride (μg/mg liver weight)
shCon
shMboat7
shCds2
shMboat7+shCds2
E
Cholesterol (μg/mg liver weight)
F
shCon
shMboat7
shCds2
shMboat7 +shCds2
G
Steatosis score
H
Upregulation
shCds2 vs shCon
shMboat7 vs shCon
536
287
673
266
256
101
387
shCds2shMboat7 vs shCon
Downregulation
shCds2 vs shCon
shMboat7 vs shCon
833
216
591
301
170
295
376
shCds2shMboat7 vs shCon
I
Downregulation
-Log10(P value)
Fatty acid metabolism
Glycine, serine and threonine metabolism
Fatty acid elongation
Lysosome
Ras signaling pathway
Biosynthesis of unsaturated fatty acids
Cholesterol metabolism
PI3K-Akt signaling pathway
Rap1 signaling pathway
ABC transporters
JAK-STAT signaling pathway
Primary bile acid biosynthesis
J
Upregulation
-Log10(P value)
Drug metabolism - other enzymes
Thermogenesis
Chemical carcinogenesis - reactive oxygen species
Alanine, aspartate and glutamate metabolism
Protein export
Oxidative phosphorylation
Steroid biosynthesis
Ribosome biogenesis in eukaryotes
Steroid hormone biosynthesis
Cell cycle
Non-alcoholic fatty liver disease
K
shCon
shMboat7
shCds2
shMboat7 + shCds2
Relative mRNA level
p=0.05
Lxr
Abcg8
Abcg5
Abca1
Srebp2
Srebp1c
Fasn
Elov12
Hadha
L
shCon
shMboat7
shCds2
shMboat7+ shCds2
MBOAT7
CDS2
LXR
f-SREBP2
n-SREBP2
HMGCR
SRB1
LDLR
GAPDH
55kDa
40kDa
55kDa
130kDa
70kDa
100kDa
180kDa
180kDa
35kDa
M
shCon
shMboat7
shCds2
shMboat7+shCds2
Relative protein level
MBOAT7
CDS2
LXR
n-SREBP2
HMGCR
SRB1
LDLR

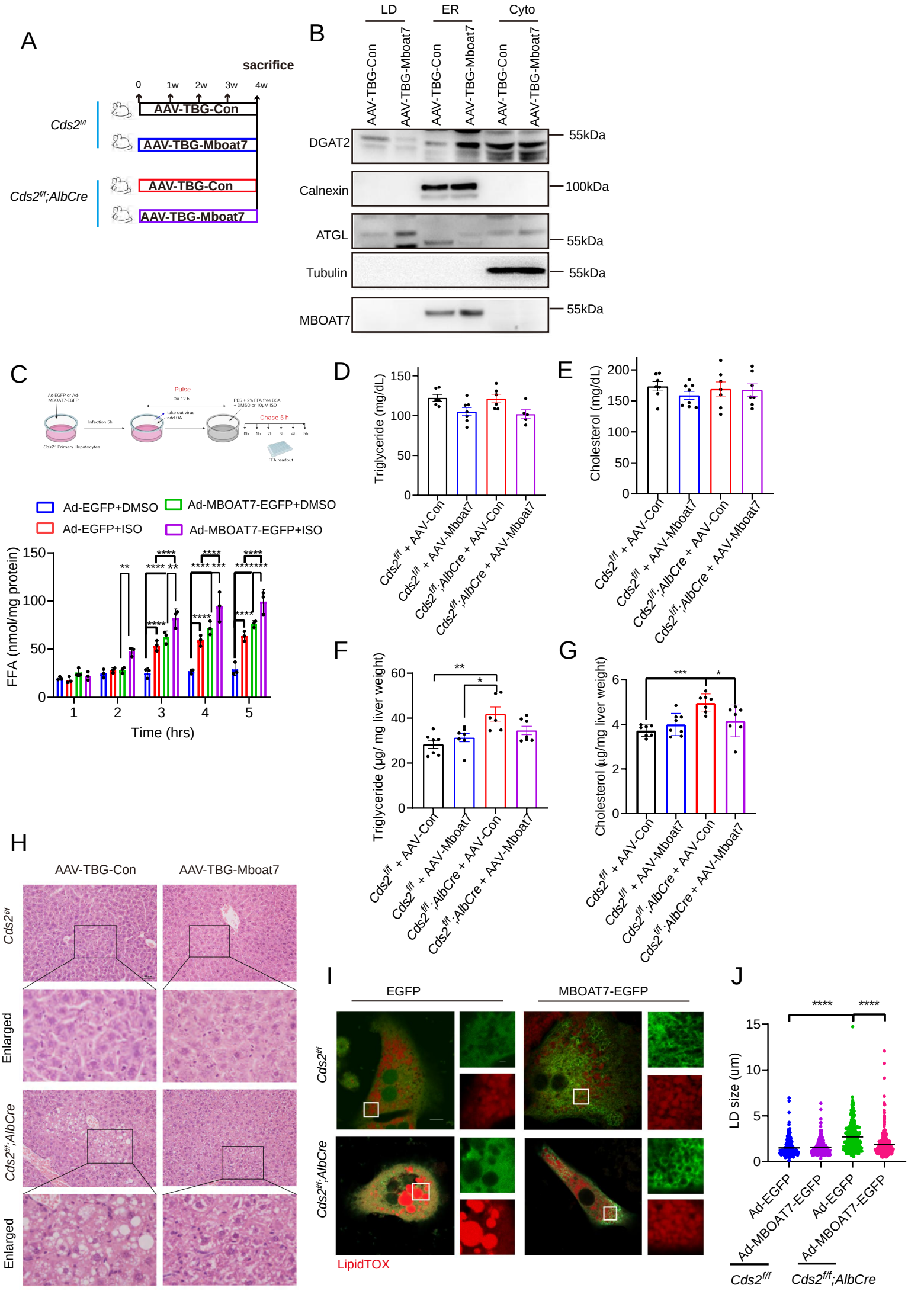
A
sacrifice
0
1w
2w
3w
4w
Cds2f/f
AAV-TBG-Con
AAV-TBG-Mboat7
Cds2f/f;AlbCre
AAV-TBG-Con
AAV-TBG-Mboat7
B
LD
ER
Cyto
AAV-TBG-Con
AAV-TBG-Mboat7
AAV-TBG-Con
AAV-TBG-Mboat7
AAV-TBG-Con
AAV-TBG-Mboat7
DGAT2
55kDa
Calnexin
100kDa
ATGL
55kDa
Tubulin
55kDa
MBOAT7
55kDa
C
Ad-EGFP or Ad-MBOAT7-EGFP
Infection 5h
Cds2f/f Primary Hepatocytes
Pulse
OA 12 h
take out virus add OA
PBS + 2% FFA free BSA + DMSO or 10μM ISO
Chase 5 h
0h
1h
2h
3h
4h
5h
FFA readout
Ad-EGFP+DMSO
Ad-MBOAT7-EGFP+DMSO
Ad-EGFP+ISO
Ad-MBOAT7-EGFP+ISO
FFA (nmol/mg protein)
Time (hrs)
D
Triglyceride (mg/dL)
Cds2f/f + AAV-Con
Cds2f/f + AAV-Mboat7
Cds2f/f;AlbCre + AAV-Con
Cds2f/f;AlbCre + AAV-Mboat7
E
Cholesterol (mg/dL)
F
Triglyceride (μg/ mg liver weight)
G
Cholesterol (μg/mg liver weight)
H
AAV-TBG-Con
AAV-TBG-Mboat7
Cds2f/f
Enlarged
Cds2f/f;AlbCre
Enlarged
I
EGFP
MBOAT7-EGFP
Cds2f/f
Cds2f/f;AlbCre
LipidTOX
J
LD size (um)
Ad-EGFP
Ad-MBOAT7-EGFP
Ad-EGFP
Ad-MBOAT7-EGFP
Cds2f/f
Cds2f/f;AlbCre

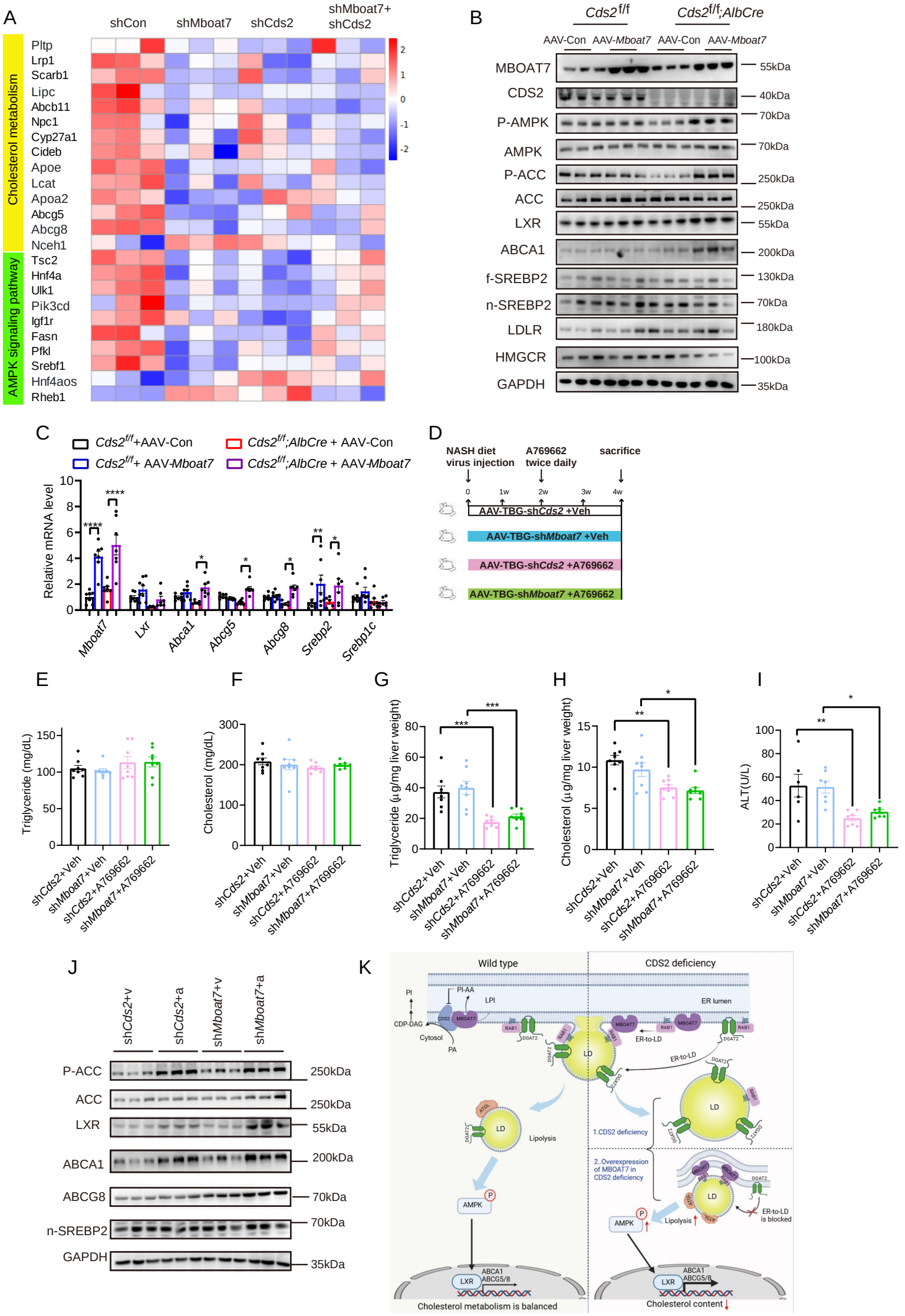
A
shCon
shMboat7
shCds2
shMboat7+ shCds2
Cholesterol metabolism
AMPK signaling pathway
Pltp
Lrp1
Scarb1
Lipc
Abcb11
Npc1
Cyp27a1
Cideb
Apoe
Lcat
Apoa2
Abcg5
Abcg8
Nceh1
Tsc2
Hnf4a
Ulk1
Pik3cd
Igf1r
Fasn
Pfkl
Srebf1
Hnf4aos
Rheb1
B
Cds2f/f
Cds2f/f;AlbCre
AAV-Con
AAV-Mboat7
MBOAT7
CDS2
P-AMPK
AMPK
P-ACC
ACC
LXR
ABCA1
f-SREBP2
n-SREBP2
LDLR
HMGCR
GAPDH
55kDa
40kDa
70kDa
250kDa
130kDa
180kDa
100kDa
35kDa
C
Cds2f/f+AAV-Con
Cds2f/f+ AAV-Mboat7
Cds2f/f;AlbCre + AAV-Con
Cds2f/f;AlbCre + AAV-Mboat7
Relative mRNA level
Mboat7
Lxr
Abca1
Abcg5
Abcg8
Srebp2
Srebp1c
D
NASH diet
virus injection
A769662
twice daily
sacrifice
0
1w
2w
3w
4w
AAV-TBG-shCds2 +Veh
AAV-TBG-shMboat7 +Veh
AAV-TBG-shCds2 +A769662
AAV-TBG-shMboat7 +A769662
E
Triglyceride (mg/dL)
F
Cholesterol (mg/dL)
G
Triglyceride (μg/mg liver weight)
H
Cholesterol (μg/mg liver weight)
I
ALT(U/L)
shCds2+Veh
shMboat7+Veh
shCds2+A769662
shMboat7+A769662
J
shCds2+v
shCds2+a
shMboat7+v
shMboat7+a
P-ACC
ACC
LXR
ABCA1
ABCG8
n-SREBP2
GAPDH
250kDa
55kDa
200kDa
70kDa
35kDa
K
Wild type
CDS2 deficiency
PI
PI-AA
LPI
CDP-DAG
Cytosol
PA
CDS2
MBOAT7
RAB1
DGAT2
LD
ER lumen
ER-to-LD
ATGL
Lipolysis
AMPK
P
1.CDS2 deficiency
2..Overexpression of MBOAT7 in CDS2 deficiency
ER-to-LD is blocked
ABCA1
ABCG5/8
LXR
Cholesterol metabolism is balanced
Cholesterol content